RNA-protein interactome at the Hepatitis E virus internal ribosome entry site

Shiv Kumar[1], Rohit Verma[1], Sandhini Saha[2], Ashish Agrahari[3], Shivangi Shukla[1], Anurag[1], Tushar Kanti Maiti[2], Shailendra Asthana[3], C.T. Ranjith-Kumar[4], Milan Surjit[1]*

[1]Virology Laboratory, Translational Health Science and Technology Institute, NCR Biotech Science Cluster, Faridabad, 121001, Haryana, India.

[2]Laboratory of functional proteomics, Regional Centre for Biotechnology, NCR Biotech Science Cluster, Faridabad, 121001, Haryana, India.

[3]Noncommunicable disease group, Translational Health Science and Technology Institute, NCR Biotech Science Cluster, Faridabad, 121001, Haryana, India.

[4]University School of Biotechnology, Guru Gobind Singh Indraprastha University, New Delhi, 110078, India.

* Correspondence: milan@thsti.res.in

Abstract

Multiple processes exist in a cell to ensure continuous production of essential proteins either through cap-dependent or cap-independent translation processes. Viruses depend on the host translation machinery for viral protein synthesis. Therefore, viruses have evolved clever strategies to utilize the host translation machinery. Earlier studies have shown that genotype 1-Hepatitis E virus (g1-HEV) utilizes both cap-dependent and cap-independent translation machineries for its replication and proliferation. Cap-independent translation in g1-HEV is driven by an eighty seven nucleotide-long RNA element which acts as a noncanonical, internal ribosome entry site like (IRESl) element. Here, we have identified the RNA-protein interactome of the HEV IRESl element and characterized the functional significance of some of its components. Our study reveals indispensable roles of host ribosomal protein RPL5 and DHX9 (RNA helicase A) in mediating efficient translation from the IRESl element and establish the function of HEV IRESl as a bonafide internal ribosome entry site.

Author summary

Protein synthesis is a fundamental process for survival and proliferation of all living organisms. Majority of cellular proteins are produced through cap-dependent translation. Cells also utilize a variety of cap-independent translation processes to synthesize essential proteins during stress. Viruses depend on the host cell translation machinery to synthesize their own proteins. Hepatitis E virus is a major cause of hepatitis worldwide. The viral genome is a capped positive strand RNA. Viral non-structural and structural proteins are synthesized through a cap-dependent translation process. An earlier study from our laboratory reported the presence of a fourth ORF in genotype 1-HEV, which produced the ORF4 protein using a cap-independent internal ribosome entry site-like (IRESl) element. In the current study, we identified the host proteins that associate with the HEV-IRESl RNA and generated the RNA-protein interactome. Through a variety of experimental approaches, our data proves that HEV-IRESl is a bonafide internal ribosome entry site.

Introduction

Protein synthesis is an essential process for survival and growth of all organisms. Viruses depend on the host cell machinery for synthesis of their proteins. Proteins are synthesized by the process of translation, which involves four distinct steps such as initiation, elongation, termination and recycling of the ribosomes. In eukaryotes, under normal conditions, majority of mRNA are translated by recognition of the m^7G (5')$_{PPP}$(5')N(cap) structure present at the 5'-end of the mRNA, by the process of cap-dependent translation. Many cellular and viral mRNAs are translated by the cap-independent mechanisms, by using distinct *cis*-acting regulatory elements, such as the cap-independent translational enhancers (CITEs), m^6A modification of the mRNAs or the internal ribosome entry sites (IRES). Initiation of the cap-dependent translation occurs through a ribosomal scanning mechanism, in which the 48S initiation complex moves along the mRNA from the m^7G cap in the 5' to 3' direction to locate a suitable AUG initiation codon. Following AUG recognition, through a series of steps, 80S ribosome complex is assembled on the mRNA with met-tRNAi bound to the AUG codon at the P-site, leading to translation elongation (1). The CITES are located in either 5'- or 3'- UTRs (untranslated regions) of the mRNAs and they initiate cap-independent translation by recruiting the initiation factors to the uncapped mRNAs, followed by 5'-end ribosomal scanning mediated identification of the initiation codon. Under conditions of stress, the cap-independent translation of many cellular mRNAs such as c-myc, Apaf-1, XIAP seem to occur through the above mechanism (2,3). A variant of the eukaryotic initiation factor 4G (eIF4G) has been shown to be important for the cap-independent translation of the c-myc mRNA (4). Recently, yeast eIF4G1 was shown to mediate the cap-independent translation from the black beatle virus 5'-untranslated region (UTR) (5). Translation of 5'- or 3'- UTR m^6A modified mRNAs also occur in a cap-independent manner (6,7,8).

Cap-independent, IRES-mediated translation has been reported in many positive-strand RNA viruses, which contain an uncapped genomic RNA. 5'-UTR in the genomic RNA of these viruses contain highly structured RNA elements, which directly recruit the initiation factors and promote translation through a scanning independent process, with the exception of the type I IRES, which depends on the ribosomal scanning process. IRES

106 have been divided into 5 major types based on their mode of ribosome recruitment and
107 RNA structure. The type I and type II IRES are found in the Picorna viruses such as the
108 Polio virus (PV) and the Foot and Mouth Disease virus (FMDV), respectively. The PV
109 IRES harbors six stem loops designated as domain I to VI. The Domain I forms unique
110 clover leaf structure and is critical for replication of both the positive and the negative
111 sense RNA. The domains II to VI are responsible for the PV IRES activity. During PV
112 infections, viral $2A^{pro}$ cleaves the eIF4E binding N-terminal domain of the eIF4G without
113 affecting its eIF3/eIF4A binding property. Stable association of the eIF4G with the PV
114 IRES domain V promotes binding of other initiation factors, leading to formation of the
115 43S preinitiation complex. The FMDV IRES is a well-studied example of the type II IRES.
116 The domain IV of the FMDV IRES binds with scaffold protein eIF4G**.** The $3C^{pro}$ and L^{pro} of
117 FMDV cleave the eIF4G similar to the $2A^{pro}$ of the type I IRES**.** Notably, the FMDV IRES
118 skips ribosomal scanning, instead, IRES proximal stem loop formation brings 84
119 nucleotides downstream AUG, close to the first AUG to start the translation by direct
120 ribosome transfer**.** Other identified cis-acting elements for the type II IRES activity are the
121 GNRA, RAAA and C-rich loop in the domain III (9). The type III IRES is present in the 5'-
122 UTR of the Hepatitis A virus genome (10). It requires eIF4E binding for translation
123 initiation (11)**.** The type IV IRES have been reported in members of the Flaviviridae family,
124 classified as the HCV (Hepatitis C virus)/ HCV-like IRES. The 5'-UTR of HCV contains
125 four domains: the domain I and II are involved in the viral replication while the domains III
126 and IV are involved in the IRES activity (12,13). The HCV/HCV-like IRES are shorter in
127 comparison to the type I and II IRES. The domains II and III contain several subdomains
128 for interaction with the 40S ribosomal subunit. The type V IRES includes the long
129 intergenic region (IGR) IRES, found between two open reading frames in the viral
130 genomes and conserved in the dicistroviridae family (12,13). The IGR IRES are the
131 smallest IRES (~180 nt long) elements consisting of three pseudoknots. It directly binds
132 to the ribosomes and initiates translation with the alanine-tRNAi (ala-tRNAi) instead of the
133 met-tRNAi, without involving the eIFs (14,15).

134 Many viruses have evolved the ability to utilize both cap-dependent and cap-independent
135 translation processes, depending on the state of the cell. Notably, although Dengue virus
136 and Zika virus genomic RNA is usually translated through a cap-dependent mechanism,

137 their 5'-UTRs also contain IRES-elements, which maintain viral translation under
138 unfavorable conditions where cap-dependent translation is inhibited by the host
139 (16,17,18). Similarly, genomic RNA of the Human Immunodeficiency Virus (HIV) type 1
140 and the Simian Immunodeficiency virus (SIV) contain IRES-elements in their 5'-leader
141 sequences, which maintain viral translation when cap-dependent translation is inhibited
142 (19,20,21,22). In addition, recent studies have identified functional IRES elements within
143 open reading frames of viral protein coding genes. For example, five functional IRES-
144 elements are located within the coding region of the non-structural and the structural
145 proteins of the human rhinovirus 16, which are active under conditions of endoplasmic
146 reticulum (ER) stress (23,24). The Human cytomegalovirus pUL138 protein is translated
147 by an IRES under conditions of stress (25). Further, coat protein of the Turnip crinkle virus
148 (TCV) is translated through an unstructured IRES (26).

149 The Hepatitis E virus is a positive strand RNA virus of the family Hepeviridae. The viral
150 genome is capped at the 5'-end followed by a short UTR of 25 nucleotides. The viral non-
151 structural proteins are synthesized from the ORF1 located between 26-5107 nucleotides.
152 Viral capsid protein is produced by the ORF2, located at the 3'-end between 5145-7127
153 nucleotides. A short 3'-UTR of 65 nucleotides is present downstream of the ORF2,
154 followed by a poly-A tail (27). A third ORF is present between the ORF1 and ORF2, which
155 produces ORF3 protein, an accessory protein that associates with the host Tumor
156 susceptibility gene 101 and facilitates release of the progeny virus (28-30). The above
157 genome organization is conserved among the 7 genotypes of the HEV. In contrast to
158 zoonotic nature of some HEV genotypes, g1-HEV infection is restricted to the human.
159 The g1-HEV does not replicate efficiently in mammalian cell lines (31).

160 Our earlier study demonstrated the coexistence of both cap-dependent and cap-
161 independent translation in the g1-HEV (32). Although HEV non-structural and structural
162 proteins are synthesized by a cap-dependent translation process, a protein essential for
163 g1-HEV replication (ORF4 protein) is synthesized from an overlapping ORF located within
164 the viral ORF1 through a cap-independent translation process. An 87-nucleotide
165 conserved RNA regulatory element located upstream of the ORF4 coding region was
166 found to drive cap-independent translation of the ORF4 protein. Interestingly, although

167 ORF4 protein production in g1-HEV infected cells was markedly enhanced upon
168 treatment of cells with ER stress-inducing compounds, HEV IRESl functioned efficiently
169 irrespective of the ER stress inducer treatment in *in-vitro* translation assays or bicistronic
170 reporter-based assays. Analysis of cap-independent translation driven by the HEV RNA
171 regulatory element by bicistronic reporter assays along with site directed mutagenesis
172 mediated mapping of the regulatory RNA sequence suggested the HEV RNA regulatory
173 element to be an IRES-element. However, considering the small size of the regulatory
174 element and its lack of strong homology with canonical IRES-elements, it was designated
175 as an IRES-like (IRESl) element. The current study was designed to further explore the
176 mechanism of HEV IRESl activity and verify its function as a bonafide internal translation
177 initiation site. Host interaction partners of the HEV IRESl were identified and their
178 importance in the IRESl-mediated translation was evaluated. Subsequent experiments
179 showed association of the HEV IRESl RNA with actively translating ribosomes, supporting
180 its role as a translation initiation element. Significance of these findings in validating the
181 role of HEV IRESl as a bonafide internal ribosome entry site is discussed.

182

183 **Results**

184 **Identification of host proteins that interact with the HEV IRESl element**

185 Two independent experimental approaches (RaPID assay and Yeast three hybrid assay)
186 were followed to identify the host proteins that interact with the HEV IRESl RNA. RNA -
187 protein interaction detection assay (RaPID assay) involves biotinylation of IRES
188 interacting proteins, followed by their identification by liquid chromatography with tandem
189 mass spectroscopy (LC-MS-MS) (33). RaPID assay was optimized in our laboratory (34).
190 87 nucleotides of the g1-HEV genome (Genbank ID: AF444002.1) corresponding to the
191 IRESl region was cloned into the pRMB vector between the BirA ligase binding stem-loop
192 (RMB-SLI, RMB-SLII) sequences (Fig. 1A, 1C). Analysis of the secondary structure of the
193 fusion RNA sequence using “Mfold” indicated that the HEV IRESl and the BirA ligase
194 binding stem-loops retained their distinct folding characteristics (Fig. 1A). An unrelated
195 sequence in the g1-HEV genome (618-738 nucleotides from the 5’-end, denoted as

196 control RNA) was also cloned into the pRMB vector to be used as a control to monitor
197 specificity of the assay. Biotin-untreated cells were used as an additional control and
198 experiments were performed two times and samples of each experiment were run in
199 triplicate.

200

Figure 1

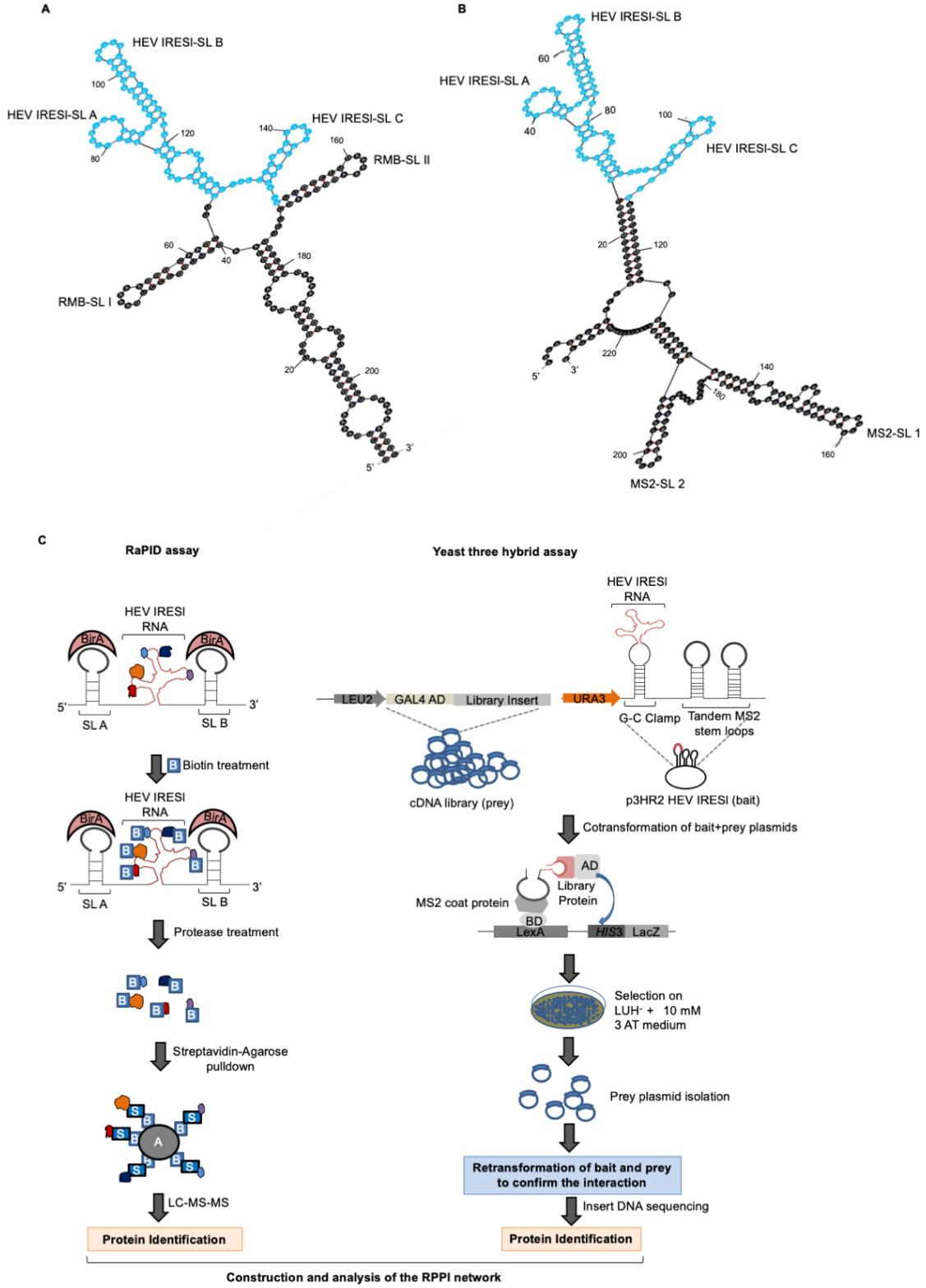
A
HEV IRESI-SL B
HEV IRESI-SL A
HEV IRESI-SL C
RMB-SL II
RMB-SL I
B
HEV IRESI-SL B
HEV IRESI-SL A
HEV IRESI-SL C
MS2-SL 1
MS2-SL 2
C
RaPID assay
HEV IRESI RNA
BirA
SL A
SL B
Biotin treatment
Protease treatment
Streptavidin-Agarose pulldown
LC-MS-MS
Protein Identification
Yeast three hybrid assay
HEV IRESI RNA
LEU2
GAL4 AD
Library Insert
URA3
G-C Clamp
Tandem MS2 stem loops
cDNA library (prey)
p3HR2 HEV IRESI (bait)
Cotransformation of bait+prey plasmids
AD
Library Protein
MS2 coat protein
BD
LexA
HIS3
LacZ
Selection on LUH⁻ + 10 mM 3 AT medium
Prey plasmid isolation
Retransformation of bait and prey to confirm the interaction
Insert DNA sequencing
Protein Identification
Construction and analysis of the RPPI network

201

202 **Figure 1. Identification of host interaction partners of the HEV IRESl element by**
203 **RaPID and Yeast three hybrid assay.**
204 (A) Schematic of predicted secondary structure of the HEV IRESl RNA (highlighted in blue) fused
205 to the BirA-binding RNA motifs (RMB-SL1 and RMB-SL2). Stem-loops of the HEV IRESl are
206 denoted as SL A, SL B, SL C (B) Schematic of predicted secondary structure of the HEV IRESl
207 RNA (highlighted in blue) fused to the MS2 coat protein-binding RNA motifs (MS2-SL1 and MS2-
208 SL2). Stem-loops of the HEV IRESl are denoted as SL A, SL B, SL C (C) Work-flow to identify
209 the HEV IRESl-binding host proteins. B: Biotin, A: Agarose, S: Streptavidin, AD: GAL4-Activation
210 domain, BD: GAL4-DNA Binding domain, L: Leucine, U: Uracil, H: Histidine, 3-AT: 3-Amino 1, 2,
211 4 Triazole, "−": Deficiency in the medium, "+": Supplemented in the medium.

212

213 Quality of the MS data between replicates of different samples was checked by Pearson
214 correlation analysis, which showed good correlation (average range: 0.2-1.0). Proteins
215 with at least one biotinylated peptide with PEP (posterior error probability) score ≥ the
216 median value in the Gaussian smoothing curve of each sample were selected for further
217 analysis. Specific interaction partners of the HEV IRESl RNA were selected by subtracting
218 the biotinylated HEV IRESl data set from the biotinylated HEV (618-738), unbiotinylated
219 HEV (618-738) and unbiotinylated HEV IRESl datasets (Fig. 2A, Fig. S1, Table S1). The
220 HEV IRESl RNA-binding protein dataset thus obtained was further analyzed to select only
221 those proteins that were represented by one or more unique peptides and a "prot score"
222 of 30 or more. Thus, a total of 43 unique proteins were identified as interaction partners
223 of the HEV IRESl RNA (Fig. 2B, Table 1).

224

Figure 2

A

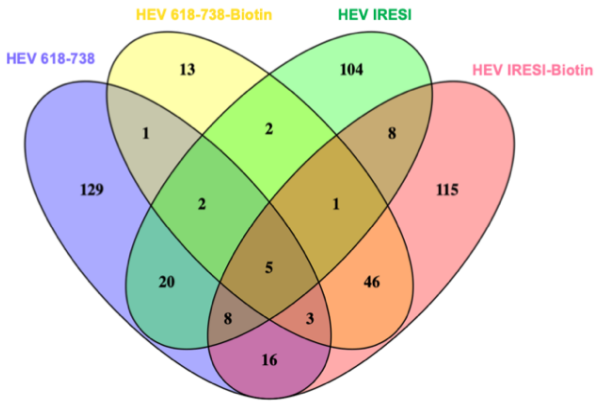

B

No. of HEV IRESI-interacting unique proteins (RaPID assay) : 43

No. of HEV IRESI-interacting unique proteins (Y3H assay) : 8

Total No. of HEV IRESI-interacting unique proteins : 51

C

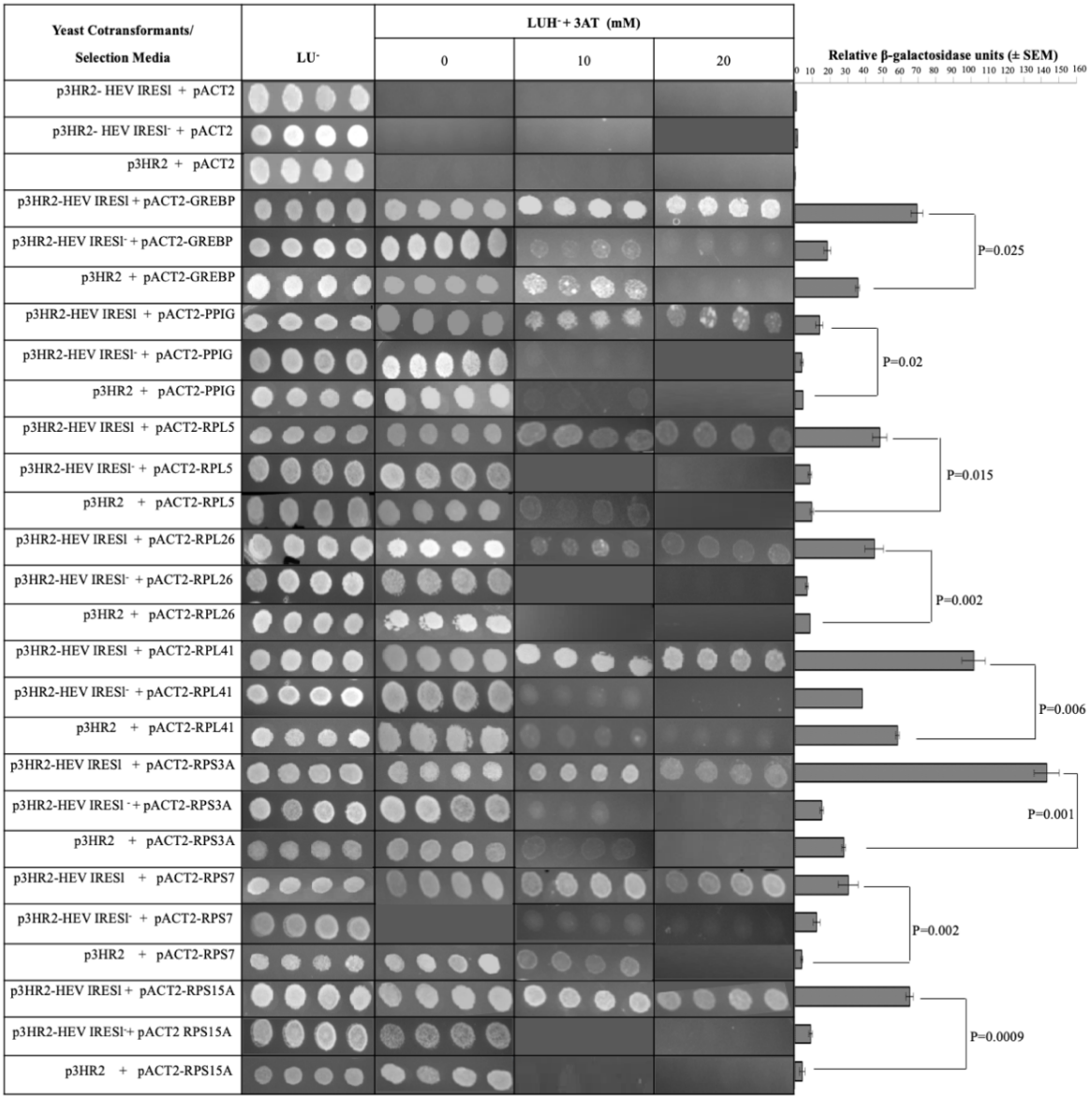

225

226 **Figure 2. Identification of HEV IRESI RNA-binding proteins by RaPID and Y3H**
227 **assay.**

228 (A) Venny analysis of the HEV IRESI RNA-binding proteins identified by the RaPID assay.
229 (B) Summary of the HEV IRESI RNA-binding proteins identified by the RaPID and the
230 Y3H assay. (C) Y3H assay mediated confirmation of the interaction between HEV IRESI
231 RNA and the host proteins identified by screening of the human liver cDNA library. YBZ1
232 strain was transformed in the indicated combinations and plated on media lacking Leucine
233 and Uracil (LU^-). Four random colonies from each cotransformant plate were replica
234 plated onto media lacking Leucine, Uracil, Histidine (LUH^-) and supplemented with 5mM
235 or 10mM 3-amino 1, 2, 4 Triazole (3-AT). Same colonies were used in liquid β-
236 galactosidase assay. Relative β-galactosidase units are plotted as mean (± SEM).

237

238

239

240

241

242

243

244

245

246

247

248

249

250 **Table 1. Host interaction partners of the HEV IRESI element**

Gene name	Description	Prot_score	No. of biotinylated peptide	No. of unique biotinylated peptide
(A) HEV IRESI-interacting host proteins, identified by the RaPID assay[a]				
EEF2	Elongation factor 2	1568	8	6
TUBA3C	Tubulin alpha-3C/D chain	929	1	1
HNRNPA2B1	Heterogeneous nuclear ribonucleoproteins A2/B1	338	2	2
DHX9	ATP-dependent RNA helicase A	285	8	7
TARS	Threonyl-tRNA synthetase, cytoplasmic	285	7	5
RPL7A	60S ribosomal protein L7a	262	4	3
BAT2L2	Protein BAT2-like 2	75	1	1
NUFIP2	Nuclear fragile X mental retardation-interacting protein 2	75	2	1
VARS	Valyl-tRNA synthetase	56	12	8
ARPP19	cAMP-regulated phosphoprotein 19	53	1	1
ENSA	Alpha-endosulfine	53	1	1
RPL24	60S ribosomal protein L24	53	1	1
TARSL2	Probable threonyl-tRNA synthetase 2, cytoplasmic	53	5	5
YTHDF2	YTH domain family protein 2	53	3	2
HSPH1	Heat shock protein 105 kDa	50	9	6
CAT	Catalase	49	2	2
DDX10	Probable ATP-dependent RNA helicase DDX10	42	15	9
LARP4	La-related protein 4	42	6	1
NDUFAF2	Mimitin, mitochondrial	41	1	1
DBNL	Drebrin-like protein	39	3	1
LBR	Lamin-B receptor	38	1	1
NSF	Vesicle-fusing ATPase	37	1	1
CEACAM16	Carcinoembryonic antigen-related cell adhesion molecule 16	35	1	1
VWA5B1	von Willebrand factor A domain-containing protein 5B1	35	5	5
CCDC65	Coiled-coil domain-containing protein 65	34	5	5
PUM1	Pumilio homolog 1	34	4	2
ARSJ	Arylsulfatase J	33	2	1
RPA1	Replication protein A 70 kDa DNA-binding subunit	33	4	4
TXLNG	Gamma-taxilin	33	17	10
AIMP1	Aminoacyl tRNA synthetase complex-interacting multifunctional protein 1	32	5	3
BIVM	Basic immunoglobulin-like variable motif-containing protein	32	7	3
CCDC67	Coiled-coil domain-containing protein 67	32	8	8
RSBN1L	Round spermatid basic protein 1-like protein	32	1	1
SH3PXD2A	SH3 and PX domain-containing protein 2A	32	1	1
UBAP2	Ubiquitin-associated protein 2	32	2	1
GLS	Glutaminase kidney isoform, mitochondrial	31	6	1
MRE11A	Double-strand break repair protein MRE11A	31	1	1
ARL6IP5	PRA1 family protein 3	31	2	1
CENPP	Centromere protein P	30	2	1
ERP29	Endoplasmic reticulum resident protein 29	30	2	1
LASP1	LIM and SH3 domain protein 1	30	1	1
TMEM59L	Transmembrane protein 59-like	30	2	1
(B) HEV IRESI-interacting host proteins, identified by the Y3H assay				
GREBP	cGMP-response Element–binding protein			
PPIG	Peptidylprolyl Isomerase G			
RPL5	Ribosomal protein L5			
RPL26	Ribosomal protein L26			
RPL41	Ribosomal protein L41			
RPS3A	Ribosomal protein S3A			
RPS7	Ribosomal protein S7			
RPS15A	Ribosomal protein S15A			

251 [a]RaPID data has been sorted on the basis of Prot score. “Bold” font represents proteins known to
252 interact with IRES elements.

253

254 Since RaPID assay may have the limitation of not identifying all proteins buried inside the
255 RNA-protein complex, yeast three hybrid (Y3H) assay was used as an alternate approach
256 to unbiasedly identify the direct interaction partners of the HEV IRESl RNA. A human liver
257 cDNA library was screened using the Y3H assay (Fig. 1C) (35, 36). In Y3H assay, the
258 bait RNA is flanked by two copies of the MS2-coat protein-binding RNA element. Analysis
259 of the RNA sequence containing fusion of the HEV-IRESl RNA and the MS2-coat protein
260 binding stem loop RNA sequences using “Mfold” indicated that their secondary structure
261 profiles remain unaltered in the fusion RNA (Fig. 1B). Self-activation of the *lacZ* and *HIS3*
262 reporter genes by the HEV IRESl RNA was checked by cotransforming the plasmids
263 encoding the HEV IRESl (p3HR2-HEV IRESl) and the GAL4 activation domain (pACT2)
264 into chemically competent YBZ1 yeast cells, followed by selection of the cotransformants
265 on the LUH^- medium and assay of the β-galactosidase activity. No growth of colonies was
266 seen on the LUH^- plates neither β-galactosidase activity was observed, indicating that
267 there was no self-activation of the reporter genes by the bait RNA (Fig. 2C). Next, the bait
268 RNA expressing YBZ1 cells were transformed with the human liver cDNA library. A total
269 of $4x10^6$ clones were screened and cotransformants were selected on the LUH^- medium
270 supplemented with 10mM 3-amino 1,2,4 triazole(3-AT). Note that 3-AT is a competitive
271 inhibitor of the Histidine biosynthesis pathway. Therefore, addition of 3-AT allows growth
272 of the cotransformants that show strong interaction between the bait RNA and the prey
273 protein. 395 colonies were obtained in the primary screening, out of which human liver
274 cDNA insert could be detected in 285 colonies (Table S2). Restriction pattern analysis of
275 the prey plasmid DNA isolated from the 285 colonies showed that unique cDNA insert
276 was present in 75 plasmids. Analysis of the cDNA insert sequences identified 8 protein
277 coding genes, which were in frame with the GAL4 activation domain (Table S2).
278 Retransformation of those 8 plasmids along with the p3HR2-HEV IRESl plasmid showed
279 that all of them were able to interact with the HEV IRESl (Fig. 2C). The eight proteins
280 include 6 ribosomal proteins (RPL5, RPL26, RPL41, RPS3A and RPS7, RPS15A), PPIG

281 (peptidylprolyl isomerase G) and GREBP (cyclic-GMP response element binding protein)
282 (Table 1).

283 Further, specificity of the interaction of eight Y3H-identified proteins with the HEV IRESl
284 was evaluated in two ways: (a) by measuring the interaction of those proteins with an
285 RNA sequence complementary to the HEV IRESl (HEV IRESl^{-}) (b) by measuring the
286 interaction of those proteins with the known IRES sequences from the genotype 3A
287 Hepatitis C virus (HCV) and the foot and mouth disease virus (FMDV). All sequences
288 were cloned into the p3HR2 vector, upstream of the MS2 coat protein-binding stem-loop
289 RNA sequences (Fig. S2). No significant interaction was observed between HEV IRESl^{-}
290 RNA and the host proteins (Fig. 2C). Y3H analysis revealed that only RPS3A interacts
291 with equal strength with all the three RNA sequences (HEV IRESl, FMDV IRES, HCV
292 IRES) (Table S3 and Fig. 3). RPL41 and RPS15A interacts exclusively with the HEV
293 IRESl RNA. While, RPL5 and RPS7 were found to interact strongly with the HEV IRESl
294 RNA and weakly with the HCV IRES. RPL26 interacts moderately and strongly with the
295 HEV IRESl and the HCV IRES, respectively, whereas it did not interact with the FMDV
296 IRES. GREBP interacts strongly with the HEV IRESl and weakly with both FMDV IRES
297 and HEV IRESl. PPIG also showed a difference in the strength of interaction among the
298 three RNA sequences in the following order- HCV IRES: strong interaction, HEV IRESl:
299 weak interaction and FMDV IRES: no interaction (Table S3 and Fig. 3).

300 In order to further ascertain that HEV IRESl interaction partners identified by RaPID and
301 Y3H are bonafide candidates, some of the interactions were further validated by an *in*
302 *vitro* pull-down assay using *in vitro* transcribed biotinylated HEV IRESl RNA as bait. Non-
303 biotinylated HEV IRESl and biotinylated control RNA (618-738 nts in g1-HEV genome) as
304 well as only cell lysate (Mock) was used as controls to ensure specificity of the assay
305 (Fig. 4A, 4B). All 10 proteins tested by the pull-down assay showed interaction with the
306 HEV IRESl RNA (Fig. 4C). Six of these interactions were originally identified by Y3H
307 assay (RPS3a, RPS7, RPL26, RPL41, PPIG, GREBP) and four were identified by RaPID
308 assay (RPL5, RPL24, LARP4, DHX9) (Fig. 4C). These data further support that the
309 proteins identified by RaPID and Y3H assay are bonafide interaction partners of the HEV
310 IRESl RNA.

Figure 3

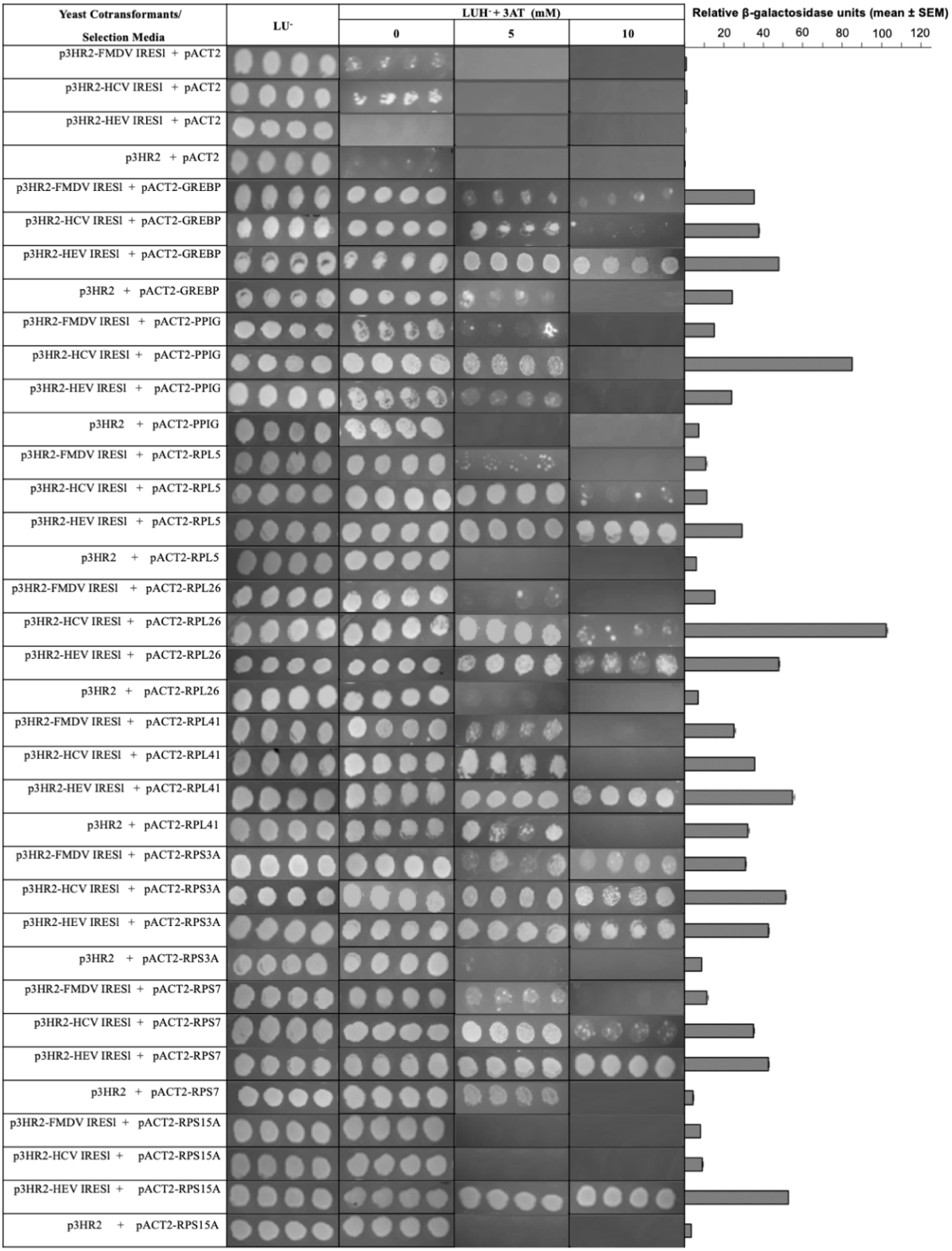
Yeast Cotransformants/
Selection Media
LU-
LUH- + 3AT (mM)
0
5
10
Relative β-galactosidase units (mean ± SEM)
20
40
60
80
100
120
p3HR2-FMDV IRESl + pACT2
p3HR2-HCV IRESl + pACT2
p3HR2-HEV IRESl + pACT2
p3HR2 + pACT2
p3HR2-FMDV IRESl + pACT2-GREBP
p3HR2-HCV IRESl + pACT2-GREBP
p3HR2-HEV IRESl + pACT2-GREBP
p3HR2 + pACT2-GREBP
p3HR2-FMDV IRESl + pACT2-PPIG
p3HR2-HCV IRESl + pACT2-PPIG
p3HR2-HEV IRESl + pACT2-PPIG
p3HR2 + pACT2-PPIG
p3HR2-FMDV IRESl + pACT2-RPL5
p3HR2-HCV IRESl + pACT2-RPL5
p3HR2-HEV IRESl + pACT2-RPL5
p3HR2 + pACT2-RPL5
p3HR2-FMDV IRESl + pACT2-RPL26
p3HR2-HCV IRESl + pACT2-RPL26
p3HR2-HEV IRESl + pACT2-RPL26
p3HR2 + pACT2-RPL26
p3HR2-FMDV IRESl + pACT2-RPL41
p3HR2-HCV IRESl + pACT2-RPL41
p3HR2-HEV IRESl + pACT2-RPL41
p3HR2 + pACT2-RPL41
p3HR2-FMDV IRESl + pACT2-RPS3A
p3HR2-HCV IRESl + pACT2-RPS3A
p3HR2-HEV IRESl + pACT2-RPS3A
p3HR2 + pACT2-RPS3A
p3HR2-FMDV IRESl + pACT2-RPS7
p3HR2-HCV IRESl + pACT2-RPS7
p3HR2-HEV IRESl + pACT2-RPS7
p3HR2 + pACT2-RPS7
p3HR2-FMDV IRESl + pACT2-RPS15A
p3HR2-HCV IRESl + pACT2-RPS15A
p3HR2-HEV IRESl + pACT2-RPS15A
p3HR2 + pACT2-RPS15A

311

312 **Figure 3. Assessment of the ability of the HEV IRESl-binding host proteins**
313 **(identified by the human liver cDNA library screening) to interact with the HCV IRES**
314 **and the FMDV IRES.**

315 YBZ1 strain was transformed in the indicated combinations and plated on media lacking
316 Leucine and Uracil (LU^-). Four random colonies from each cotransformant plate were
317 replica plated onto media lacking Leucine, Uracil, Histidine (LUH^-) and supplemented with
318 5mM or 10mM 3-amino 1, 2, 4 Triazole (3-AT). Same colonies were used in liquid β-
319 galactosidase assay. Relative β-galactosidase units are plotted as mean (± SEM).

320

321

Figure 4

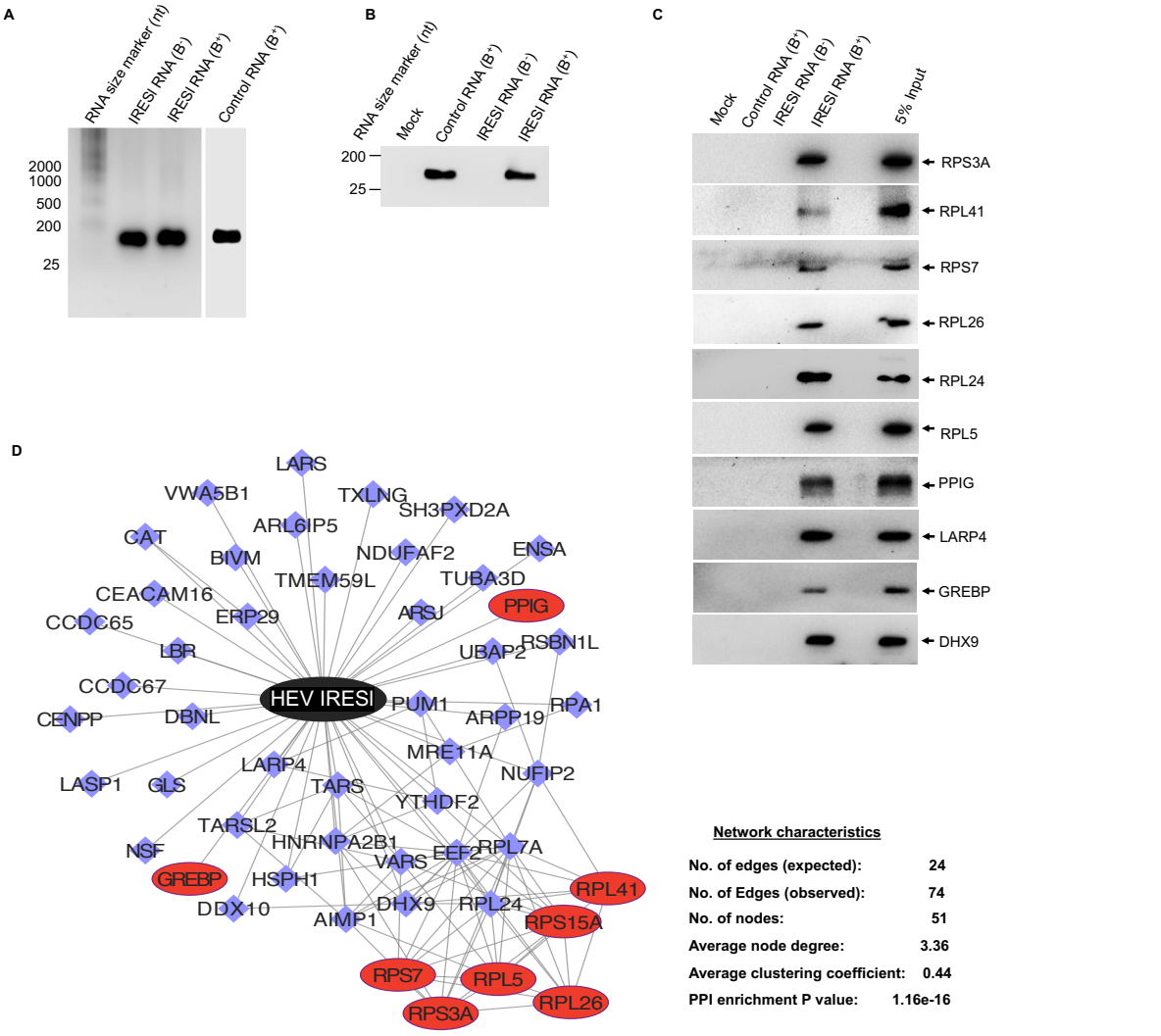
A
RNA size marker (nt)
IRESI RNA (B-)
IRESI RNA (B+)
Control RNA (B+)
2000
1000
500
200
25
B
RNA size marker (nt)
Mock
Control RNA (B+)
IRESI RNA (B-)
IRESI RNA (B+)
200
25
C
Mock
Control RNA (B+)
IRESI RNA (B-)
IRESI RNA (B+)
5% Input
RPS3A
RPL41
RPS7
RPL26
RPL24
RPL5
PPIG
LARP4
GREBP
DHX9
D
HEV IRESI
LARS
VWA5B1
TXLNG
SH3PXD2A
ARL6IP5
CAT
BIVM
NDUFAF2
ENSA
TMEM59L
TUBA3D
CEACAM16
CCDC65
ERP29
ARSJ
PPIG
LBR
UBAP2
RSBN1L
CCDC67
CENPP
DBNL
PUM1
ARPP19
RPA1
MRE11A
LASP1
GLS
LARP4
TARS
NUFIP2
YTHDF2
TARSL2
NSF
HNRNPA2B1
VARS
EEF2
RPL7A
GREBP
HSPH1
RPL41
DDX10
DHX9
RPL24
AIMP1
RPS15A
RPS7
RPL5
RPS3A
RPL26
Network characteristics
No. of edges (expected): 24
No. of Edges (observed): 74
No. of nodes: 51
Average node degree: 3.36
Average clustering coefficient: 0.44
PPI enrichment P value: 1.16e-16
E
SRP-dependent cotranslational protein targeting to membrane (GO:0006614) *5.63e-11
cytoplasmic translation (GO:0002181) *7.35e-11
cotranslational protein targeting to membrane (GO:0006613) *8.02e-11
translation (GO:0006412) *1.13e-10
protein targeting to ER (GO:0045047) *1.69e-10
nuclear-transcribed mRNA catabolic process, nonsense-mediated decay (GO:0000184) *3.56e-10
cellular macromolecule biosynthetic process (GO:0034645) *4.65e-09
peptide biosynthetic process (GO:0043043) *6.26e-09
nuclear-transcribed mRNA catabolic process (GO:0000956) *9.58e-09
ncRNA processing (GO:0034470) *3.38e-08
0
2
4
6
8
10
−log10(p-value)
F
Peptide chain elongation Homo sapiens R-HSA-156902 *5.7e-13
Eukaryotic Translation Elongation Homo sapiens R-HSA-156842 *9.75e-13
Selenoamino acid metabolism Homo sapiens R-HSA-2408522 *7.44e-12
Viral mRNA Translation Homo sapiens R-HSA-192823 *3.20e-11
Selenocysteine synthesis Homo sapiens R-HSA-2408557 *4.27e-11
Eukaryotic Translation Termination Homo sapiens R-HSA-72764 *4.27e-11
Nonsense Mediated Decay (NMD) independent of the Exon Junction Complex (EJC) Homo sapiens R-HSA-975956 *5.14e-11
Formation of a pool of free 40S subunits Homo sapiens R-HSA-72689 *9.52e-11
Translation Homo sapiens R-HSA-72766 *1.21e-10
Nonsense-Mediated Decay (NMD) Homo sapiens R-HSA-927802 *2.13e-10
0
2
4
6
8
10
12
−log10(p-value)

322

323 **Figure 4. Confirmation of HEV IRESl RNA-protein interactions by biotinylated-RNA**
324 **pull down assay and construction of the RNA-protein interaction network.**

325 (A) Formaldehyde-agarose gel electrophoresis and ethidium bromide staining mediated
326 visualization of *in vitro* transcribed and purified non-biotinylated IRSEl RNA [IRESl RNA
327 (B^-)], biotinylated IRSEl RNA [IRESl RNA (B^+)] and biotinylated control RNA [control RNA
328 (B^+)], as indicated. RNA size marker was resolved in parallel (lane 1). (B) Formaldehyde-
329 agarose gel electrophoresis and ethidium bromide staining mediated visualization of
330 eluates from streptavidin-pull down of samples containing the control RNA (B^+), IRESl
331 RNA (B^-) and IRESl RNA (B^+), as indicated. (C) Western blot analysis of the indicated
332 proteins using aliquots of eluates from biotinylated-RNA pull down of samples containing
333 the control RNA (B^+), IRESl RNA (B^-) and IRESl RNA (B^+), as indicated. 5% input denotes
334 5% of the cell lysate used for incubation with the RNAs during the pull-down assay. (D)
335 Schematic of the HEV IRESl RNA-protein interaction network. Black node denotes HEV
336 IRESl RNA, blue and red nodes denote host proteins identified by the RaPID and the Y3H
337 assay, respectively. Edges are represented by blue lines (E) Graphical representation of
338 the top 10 Biological processes (sorted by *P*-values) enriched in the HEV IRESl RNA-
339 protein interactome (F) Graphical representation of the top 10 Reactome pathways
340 (sorted by *P*-values) enriched in the HEV IRESl RNA-protein interactome.

341

342 **Construction of the HEV IRESl RNA-host protein interaction network and analysis**
343 **of the interactome.**

344 43 and 8 host proteins identified as interaction partners of the HEV-IRESl RNA by RaPID
345 and Y3H assay, respectively, were clubbed and imported to Cytoscape to generate the
346 RNA-Protein-Protein interaction (RPPI) network, as described earlier (29). Analysis of the
347 different network characteristics revealed that the HEV IRESl-RPPI network contained 51
348 nodes and 74 edges, the average node degree being 3.36. Average clustering coefficient
349 was 0.44 and the PPI enrichment P-value was $1.11e^{-16}$ (Fig. 4D). Above network
350 parameters suggest that the HEV IRESl-RPPI network is highly connected and suitable
351 for further downstream studies.

352 Next, Gene ontology (GO) and Reactome pathway analysis of the HEV IRESl-RPPI
353 network was performed using the "Enrichr" tool to determine the significantly enriched
354 processes/pathways. Proteins involved in translation and mRNA catabolic processes
355 were enriched in the GO biological processes category, supporting involvement of the
356 HEV IRESl element in the protein synthesis process (Fig. 4E, top 10 biological processes
357 are shown). Similarly, top Reactome pathways include translation, eukaryotic translation
358 elongation and seleno animo acid metabolism (Fig. 4F, top 10 Reactome pathways are
359 shown). Analysis of the dataset using the gene set enrichment analysis (GSEA) tool also
360 showed translation and peptide metabolic process as top hits, in agreement with the
361 "Enrichr" output (Fig. S3A, S3B). Components of both small and large subunits of the
362 ribosome such as RPS7, RPS3A, RPS15A and RPL5, RPL24, RPL26, RPL41 interact
363 with the HEV IRESl. Components of the tRNA synthetase complex such as Threonyl-
364 tRNA synthetase (TARS), Valyl-tRNA synthetase (VARS), Aminoacyl tRNA synthetase
365 complex-interacting multifunctional protein 1 (AIMP1) and a component of the translation
366 elongation complex (EEF2, eukaryotic elongation factor 2) also interact with the HEV
367 IRESl, further supporting its involvement in the protein synthesis process (Table 1). In
368 addition, a literature search of IRES-binding host proteins revealed that four proteins
369 identified in our study are known to bind other IRES. DHX9 and RPA1 bind to the IRES
370 of HCV and FMDV; RPS3A associates with the HCV IRES, while RPL26 interacts with
371 the p53 IRES (Table 1, highlighted in bold font) (37, 38, 39).

372

373 **Interrogation of the interaction between the HEV IRESl RNA and the host ribosomal**
374 **proteins by *in silico* analyses.**

375 *In silico* molecular docking has been used in determining the complex structures of RNA-
376 proteins interactions (40). We used HDOCK, a web-based tool which is a hybrid docking
377 algorithm of template-based modeling for determining the interaction between the HEV
378 IRESl RNA and four of the identified proteins (RPL5, RPL 26, RPS3A and RPS7) (41).
379 HEV IRESl showed direct interaction with RPL5, RPL26, RPS3A and RPS7 proteins (Fig.
380 5A-5D). All four complexes were analyzed for identification of the hot-spot residues and
381 was compared based on interaction mapping and binding energy analysis. All four

382 complexes were quantified in terms of their interaction by mapping the critical polar
383 contacts. The key nucleotides of each complex were mapped and, notably, RPS3A,
384 RPL26 and RPL5 were found to interact with the HEV IRESl through a combination of
385 common and unique nucleotides. The nucleotides U60, U29, G30 and U59 were common
386 in at least two complexes. The unique nucleotides which contribute significantly in RPL5
387 are G50 and C44; U22, G51 and C68 in RPS3A; A38, C41 and U66 in RPL26; U9, C10,
388 G12, G53 and G56 in RPS7 (Fig. 5E-5H). We also quantified the overall contributions by
389 measuring the surface contacts between the HEV IRESl nucleotides and proteins (Fig.
390 S3C). Here, the main focus was to identify the common nucleotides, which were involved
391 in contacts with the amino acids of the different ribosomal proteins. Interestingly, we found
392 that nucleotides A8, U9, C28, G51, G52, U59, U60, G61, U67, C68 and C69 were
393 common in at least three proteins. Nucleotides U29, G30, G31, A38, C41, A42, G50, C55,
394 A57, U62 and A85 were common among two proteins (Fig. S3C). Among the identified
395 nucleotides, some are engaged with two or more amino acids such as C10, U22, U29,
396 G30, U59 and U60, indicating their importance in mediating the interaction of the HEV
397 IRESl RNA with the respective ribosomal protein (Fig. 5E-5H). Further investigation of the
398 binding energy of each complex, the order of binding affinity between the four complexes
399 are RPL5 (-391.48 kcal/mol), RPL26 (-363.43 kcal/mol), RPS3A (-341.19 kcal/mol) and
400 RPS7 (-302.44 kcal/mol) (Fig. 5I). Physico-chemical analysis of the interacting amino
401 acids, it was observed that most of the interacting residues were either basic (K/R) or
402 aromatic (Y/F/H) in nature and each complex involves at least one serine residue.

403

Figure 5

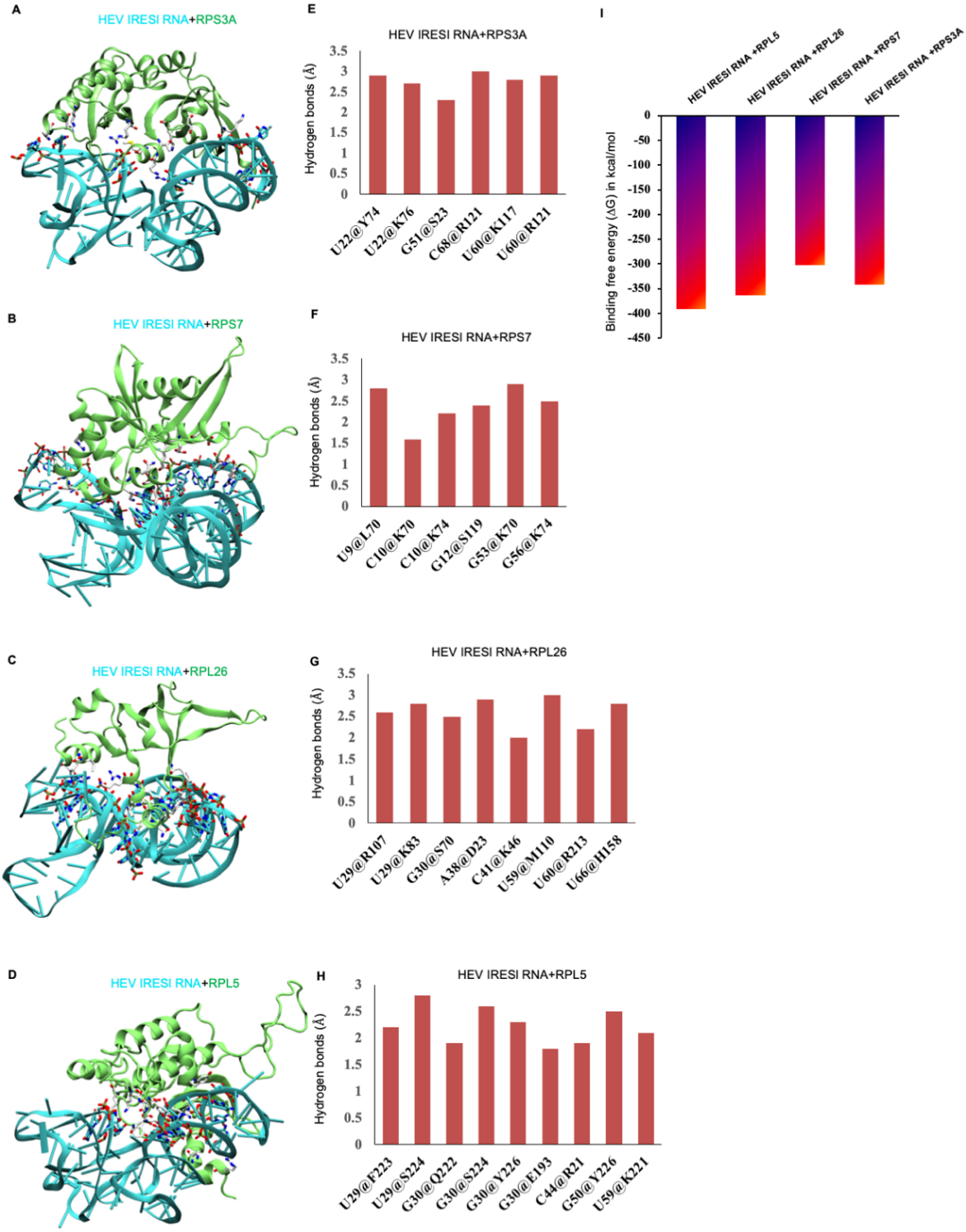
A
HEV IRESI RNA+RPS3A
E
HEV IRESI RNA+RPS3A
Hydrogen bonds (Å)
U22@Y74
U22@K76
G51@S23
C68@R121
U60@K117
U60@R121
I
HEV IRESI RNA +RPL5
HEV IRESI RNA +RPL26
HEV IRESI RNA +RPS7
HEV IRESI RNA +RPS3A
Binding free energy (ΔG) in kcal/mol
B
HEV IRESI RNA+RPS7
F
HEV IRESI RNA+RPS7
Hydrogen bonds (Å)
U9@L70
C10@K70
C10@K74
G12@S119
G53@K70
G56@K74
C
HEV IRESI RNA+RPL26
G
HEV IRESI RNA+RPL26
Hydrogen bonds (Å)
U29@R107
U29@K83
G30@S70
A38@D23
C41@K46
U59@M110
U60@R213
U66@H158
D
HEV IRESI RNA+RPL5
H
HEV IRESI RNA+RPL5
Hydrogen bonds (Å)
U29@F223
U29@S224
G30@Q222
G30@S224
G30@Y226
G30@E193
C44@R21
G50@Y226
U59@K221

404

405 **Figure 5. *In silico* mapping of the interaction between the HEV IRESI RNA and the**
406 **ribosomal proteins.**

407 (A) The interaction between the HEV IRESI and RPS3A is shown in the cartoon and
408 rendered in cyan and lime, respectively. The interacting nucleotides and amino acids are
409 rendered in licorice and colored in atom-wise mode like C: cyan/white, O: red, N: blue
410 and S: yellow. (B) The interaction between the HEV IRESI and RPS7 is shown in the
411 cartoon and rendered in cyan and lime, respectively. The interacting nucleotides and
412 amino acids are rendered as shown in (A). (C) The interaction between the HEV IRESI
413 and RPL26 is shown in the cartoon and rendered in cyan and lime, respectively. The
414 interacting nucleotides and amino acids are rendered as shown in (A). (D) The interaction
415 between the HEV IRESI and RPL5 is shown in the cartoon and rendered in cyan and
416 lime, respectively. The interacting nucleotides and amino acids are rendered as shown in
417 (A). (E-H) The quantitative polar contacts between nucleotide and amino acids are
418 measured for the indicated complexes and shown in bar-graph (Y-axis: hydrogen bond
419 distance, X-axis interacting pair of nucleotides@aminoacids). (I) The binding free energy
420 for the indicated complexes are plotted in the bar graph.

421

422 **RPL5 and DHX9 (RNA helicase A) proteins are essential for the function of the HEV**
423 **IRESI.**

424 In order to further examine the functional significance of host interaction partners of the
425 HEV IRESI, we used siRNA against some of the host factors to deplete them in the Huh7
426 cells, followed by measurement of HEV IRESI activity and g1-HEV replication. 72 hours
427 treatment of Huh7 cells with the siRNAs against RPL5, RPL24, RPL26, RPL41, RPS3A
428 and DHX9 depleted the corresponding proteins (Fig. 6A). Note that in the case of RPS3A
429 siRNA, there was a significant reduction in the GAPDH protein level at 72 hours treatment
430 period (Fig. 6A). Effect of siRNA treatment on viability of the Huh7 cells was measured at
431 72 hours post treatment. RPS3A siRNA treatment led to a significant loss of cell viability
432 (Fig. 6B). Therefore, RPS3A siRNA was excluded from further studies.

433 Next, a bicistronic reporter construct (pRL-FF/Luc dual luciferase construct) was used to
434 simultaneously measure the HEV IRESI activity (by measuring Firefly-Luc activity) and
435 cap-dependent translation activity (by measuring Renilla-Luc activity) in siRNA treated
436 Huh7 cells, as described earlier (32) (Fig. 6C). Among the ribosomal proteins, siRNAs
437 against RPL5 and RPL26 significantly reduced the activity of both Firefly-Luc (measure
438 HEV IRESI activity) and Renilla-Luc (measure cap-dependent translation activity) (Fig.
439 6D, 6E). Lack of RPL24 and RPL41 did not affect the Firefly-Luc or Renilla-Luc activity
440 (Fig. 6D, 6E). DHX9 siRNA significantly decreased the activity of both Firefly-Luc and
441 Renilla-Luc (Fig. 6D, 6E). Next, g1-HEV expressing Huh7 cells were treated with different
442 siRNAs, followed by measurement of the level of viral sense strand RNA. Lack of RPL5
443 and DHX9 proteins significantly reduced the level of g1-HEV RNA (Fig. 6F). However,
444 lack of RPL24 and RPL26 did not affect g1-HEV RNA level and lack of RPL41 marginally
445 enhanced the level of g1-HEV RNA (Fig. 6F).

446

Figure 6

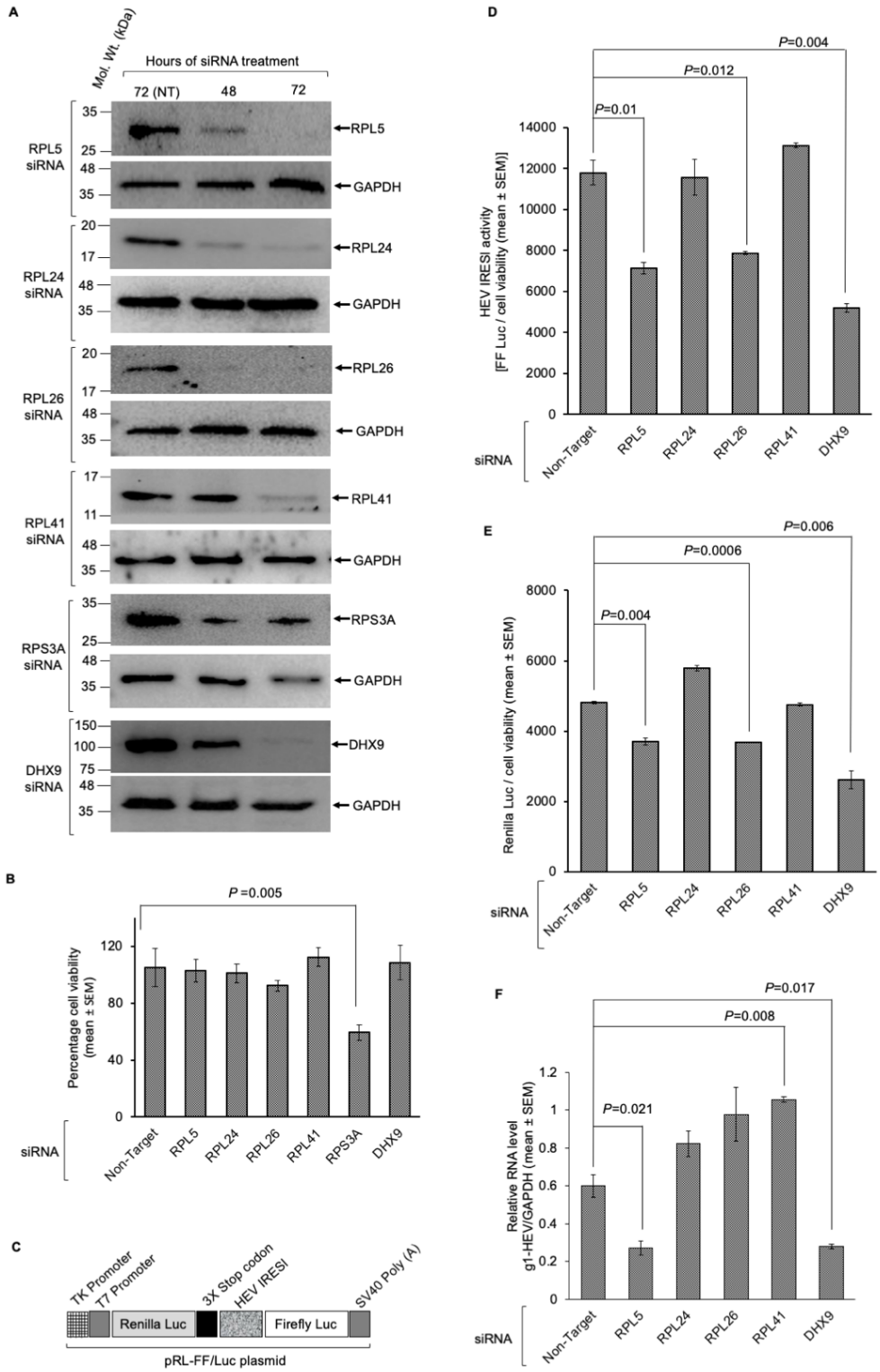
A
Mol. Wt. (kDa)
Hours of siRNA treatment
72 (NT)
48
72
RPL5 siRNA
RPL24 siRNA
RPL26 siRNA
RPL41 siRNA
RPS3A siRNA
DHX9 siRNA
RPL5
RPL24
RPL26
RPL41
RPS3A
DHX9
GAPDH
B
P =0.005
Percentage cell viability (mean ± SEM)
siRNA
Non-Target
RPL5
RPL24
RPL26
RPL41
RPS3A
DHX9
C
TK Promoter
T7 Promoter
3X Stop codon
HEV IRESI
SV40 Poly (A)
Renilla Luc
Firefly Luc
pRL-FF/Luc plasmid
D
P=0.004
P=0.012
P=0.01
HEV IRESI activity [FF Luc / cell viability (mean ± SEM)]
E
P=0.006
P=0.0006
P=0.004
Renilla Luc / cell viability (mean ± SEM)
F
P=0.017
P=0.008
P=0.021
Relative RNA level g1-HEV/GAPDH (mean ± SEM)

447

448 **Figure 6. Essential roles of the ribosomal protein RPL5 and RNA helicase DHX9 in**
449 **mediating the function of the HEV IRESl element.**

450 (A) Western blot analysis of the indicated proteins after 48- and 72-hours treatment with
451 the indicated siRNAs (lanes 2 and 3). Lane 1 shows protein from cells treated for 72 hours
452 with a non-target siRNA (NT) (B) Percent viability of Huh7 cells treated with the indicated
453 siRNAs for 72 hours. The value for the non-target siRNA treated cells was considered to
454 be 100% and other values were calculated relative to that. Values are the mean (± SEM)
455 of triplicate samples (C) Schematic of the pRL-FF/Luc bicistronic reporter plasmid (D)
456 Firefly-Luciferase activity of Huh7 cells transfected with the indicated siRNAs and the
457 pRL-FF/Luc plasmid for 72 hours. The Firefly-Luc values were divided by that of the cell
458 viability and represented as mean (± SEM) of triplicate samples (E) The Renilla-
459 Luciferase activity of the Huh7 cell lysate used in (C). The Renilla-Luc values were divided
460 by that of the cell viability and represented as mean (± SEM) of triplicate samples (F) RT
461 q-PCR measurement of intracellular level of the g1-HEV genomic RNA in the Huh7 cells
462 transfected with the indicated siRNAs for 72 hours. Values for the g1-HEV RNA was
463 normalized to that of the GAPDH RNA and represented as mean (± SEM) of triplicate
464 samples.

465

466 **HEV IRESl RNA is associated with the polysomes in translationally active cells.**

467 A ribosomal fractionation assay was performed to verify the localization of the HEV IRESl
468 element in actively translating ribosomes (Fig. 7A). A construct expressing the Firefly-Luc
469 reporter under control of the HEV IRESl in a cap-independent manner (pSuper-HEV
470 IRESl) was used to distinctly identify the presence of the HEV IRESl in the actively
471 translating ribosomes. Note that HEV IRESl RNA transcription is driven by the H1 RNA
472 polymerase III promoter in the pSuper vector. A Renilla-Luc reporter driven by cap-
473 dependent translation was used as a positive control for the assay (pRL-TK). HEK 293T
474 cells were cotransfected with the pSuper-HEV IRESl and the pRL-TK plasmids. 48 hours
475 post transfection, cells were lysed and Firefly, Renilla-Luc activity was measured. As
476 expected, significant activity of both Firefly and Renilla-Luc was observed (Fig. 7B). In

477 order to verify if Firefly-Luc was produced through a cap-independent process, total RNA
478 was isolated from the cotransfected cells, followed by immunoprecipitation of capped
479 RNAs using the anti-m^7G cap antibody, which specifically recognizes the m^7G in the cap
480 structure (42). Level of the Firefly or the Renilla-Luc encoding RNA was quantified by
481 Real-Time PCR. As expected, the Renilla-Luc RNA was detected in the anti-m^7G cap
482 antibody immunoprecipitated sample whereas the Firefly-Luc RNA was not detectable in
483 aliquots of the same sample (Fig. 7C). In contrast, the Firefly-Luc RNA was detected in
484 the unbound fraction only (Fig. 7C).

485 Next, cytoplasmic fractions of HEK 293T cells cotransfected with the pSuper-HEV IRESl
486 and the pRL-TK plasmids were subjected to linear (10-50%) sucrose density gradient
487 centrifugation, followed by measurement of both Firefly and Renilla-Luc RNAs in different
488 fractions. Cells were lysed after treatment with cycloheximide (CHX) or puromycin (Puro),
489 which stalls translating ribosomes or prevents the polysome assembly, respectively (43,
490 44). Ribosome profiles of cycloheximide and puromycin treated cells showed an expected
491 pattern, in agreement with the earlier studies (Fig. S4A) (44). Total RNA was isolated from
492 aliquots of the alternate fractions from the density gradient samples and resolved by
493 formaldehyde-agarose gel electrophoresis, followed by visualization of 28S and 18S RNA
494 by ethidium bromide staining. As expected, 28S and 18S RNA was majorly present in the
495 fractions corresponding to the polysomes in the cycloheximide treated samples (Fig. S4B,
496 upper panel), which was significantly reduced in the puromycin treated samples (Fig.
497 S4B, lower panel). RT-qPCR revealed that in cycloheximide treated cells both Firefly and
498 Renilla-Luc RNA were predominantly detected in the fractions 9 onwards, indicating their
499 association with the polysomes (Fig. 7D). On the other hand, control RNA was mostly
500 present in fractions 1 and 3 (representing free RNA), indicating its inability to associate
501 with the polysome, which further confirms the specificity of the ribosome fractionation
502 assay (Fig. 7D). Next, aliquots of the density gradient fractions were used for western blot
503 analysis of the different ribosomal proteins, DHX9 and PPIG. In cycloheximide treated
504 cells, RPS3A, RPL26, RPS7, RPL5 and RPL24 were predominantly present in the
505 polysome fractions (Fig. 7E). DHX9 was found in both 40S-80S ribosome-containing
506 fractions and polysome fractions (Fig. 7E). PPIG was predominately found in the free
507 mRNA or 40S-80S ribosome complex-containing fractions (Fig. 7E). PPIG was used as

508 a control to monitor purity of the polysome fractions as it is not known to be present in the
509 polysomes. Note that PPIG is a peptidyl-prolyl isomerase of the cyclophilin family, which
510 catalyze the conversion between *cis* and *trans* isomers of proline (45). Collectively, these
511 findings confirm that the HEV IRESI RNA is complexed with actively translating
512 ribosomes.

Figure 7

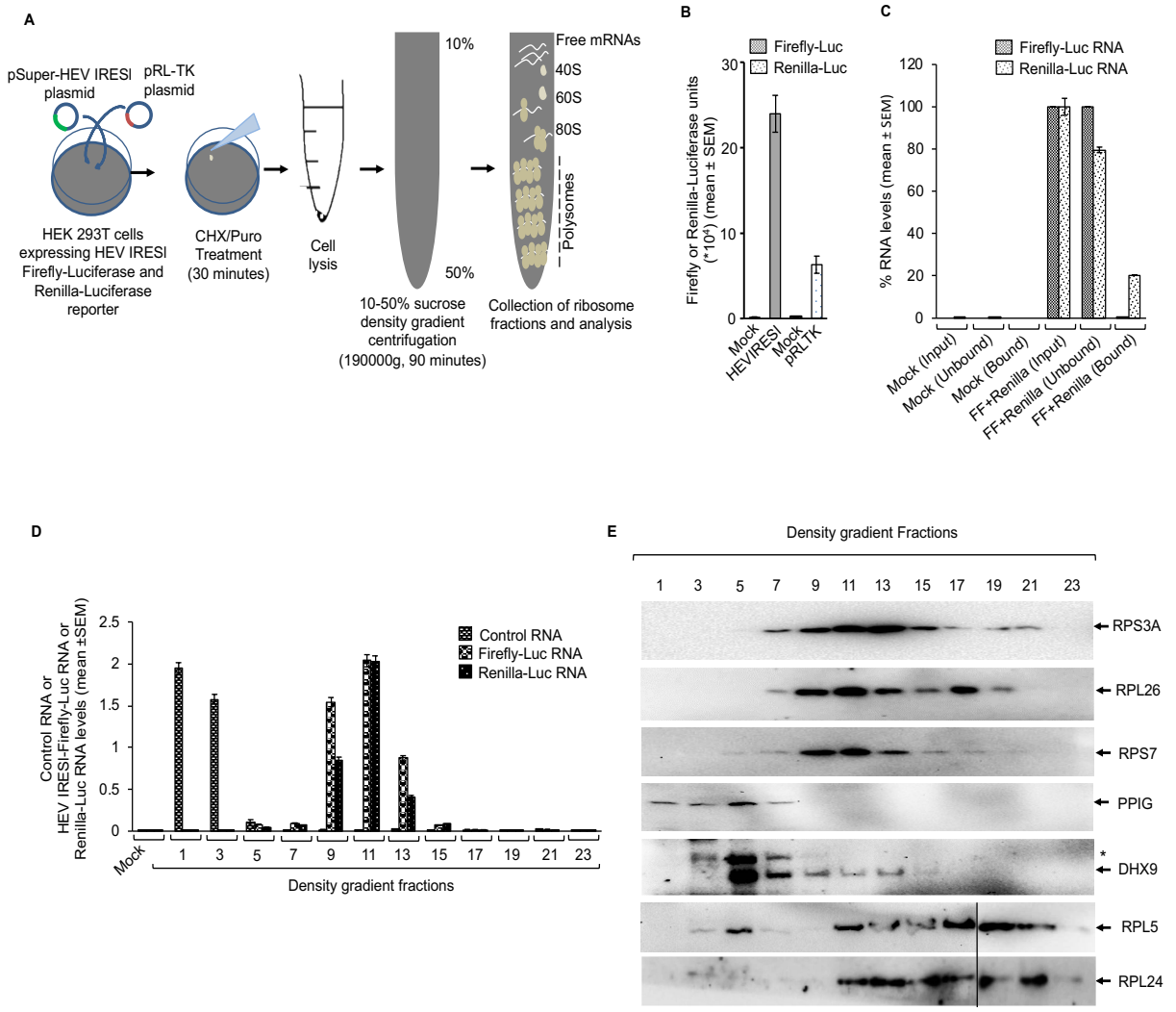

513

514

515 **Figure 7. The HEV IRESI element associates with actively translating ribosomes.**

516 (A) Schematic of the ribosome fractionation assay. CHX: Cycloheximide, Puro: Puromycin
517 (B) Measurement of the Firefly and the Renilla-Luciferase activities in the Huh7 cells,
518 cotransfected with the pSuper-HEV IRESl and the pRL-TK plasmids. Mock shows pSuper
519 vector transfected Huh7 cells, processed in parallel. Values are represented as mean (±
520 SEM) of triplicate samples (C) RT-qPCR analysis of the Firefly-Luc and the Renilla-Luc
521 RNAs obtained by the RNA-IP assay using anti- m^7G-cap antibody. Mock: RNA from the
522 pSuper vector transfected Huh7 cells, FF+Renilla: RNA from the Huh7 cells cotransfected
523 with the pSuper-HEV IRESl and pRL-TK plasmids, Input: amount of RNA used for RNA-
524 IP, Unbound: RNA isolated from supernatant of the IP samples before washing, Bound:
525 RNA isolated from the elution fraction of the IP samples. Values are shown as mean (±
526 SEM) of triplicate samples. (D) RT-qPCR analysis of the Control RNA, Firefly-Luc RNA
527 and the Renilla-Luc RNA levels in aliquots of the total RNA isolated from the sucrose
528 density gradient fractions of the Huh7 cells, cotransfected with the pSuper-control RNA
529 plasmid, pSuper-HEV IRESl plasmid and pRL-TK plasmid and treated with
530 cycloheximide. Values are mean (± SEM) of triplicate samples. (E) Western blot analysis
531 of the level of indicated proteins present in the density gradient fractions, as shown in (D).
532 "*": non-specific band detected by the anti-DHX9 antibody.

533

534 Importance of the HEV IRESl RNA-binding translation-related proteins in driving the
535 association of the HEV IRESl RNA with the polysomes was further assessed by a
536 ribosome fractionation assay in Firefly and Renilla-Luc expressing, different siRNA and
537 cycloheximide-treated HEK 293T cells. Fractions 1, 5, 9 and 13 from the density gradient
538 centrifugation samples were analyzed to quantify the levels of Firefly and Renilla-Luc
539 RNAs as free RNA (fraction 1), in 40S-60S ribosome complex (fraction 5) or the polysome
540 complex (fractions 9 and 13). Treatment of cells with siRNAs against RPL5, RPL26 and
541 DHX9 significantly reduced the HEV IRESl RNA association with the polysomes whereas
542 siRNAs against RPL24 and RPL41 did not affect that (Fig. 8A). However, in the case of
543 Renilla-Luc RNA, in addition to RPL5 and RPL26, treatment with RPL24 siRNA also
544 significantly reduced the association of the Renilla-Luc RNA with the polysomes. Further,
545 treatment with DHX9 or RPL41 siRNAs did not affect the association of the Renilla-Luc

546 RNA with the polysomes (Fig. 8B). Next, aliquots of the above samples were analyzed
547 for detection of the RPL5 protein (an indicator of polysome-containing fractions). As
548 expected, RPL5 was predominately detected in the polysome-containing fractions (Fig.
549 8C, non-Target siRNA). Treatment with RPL5 siRNA significantly reduced its level.
550 Treatment with RPL24 siRNA also decreased the level of polysomes whereas RPL26,
551 RPL41 and DHX9 siRNA treatment did not affect the polysomes (Fig. 8C). Collectively,
552 these findings confirm the association of the HEV IRESI RNA with actively translating
553 ribosomes and suggest that RPL5 and DHX-9 help in HEV IRESI-mediated translation by
554 holding the RNA in the polysomes whereas DHX9 is dispensable for holding the Renilla-
555 Luc RNA (cap-dependent translation) in the polysomes.

556

Figure 8

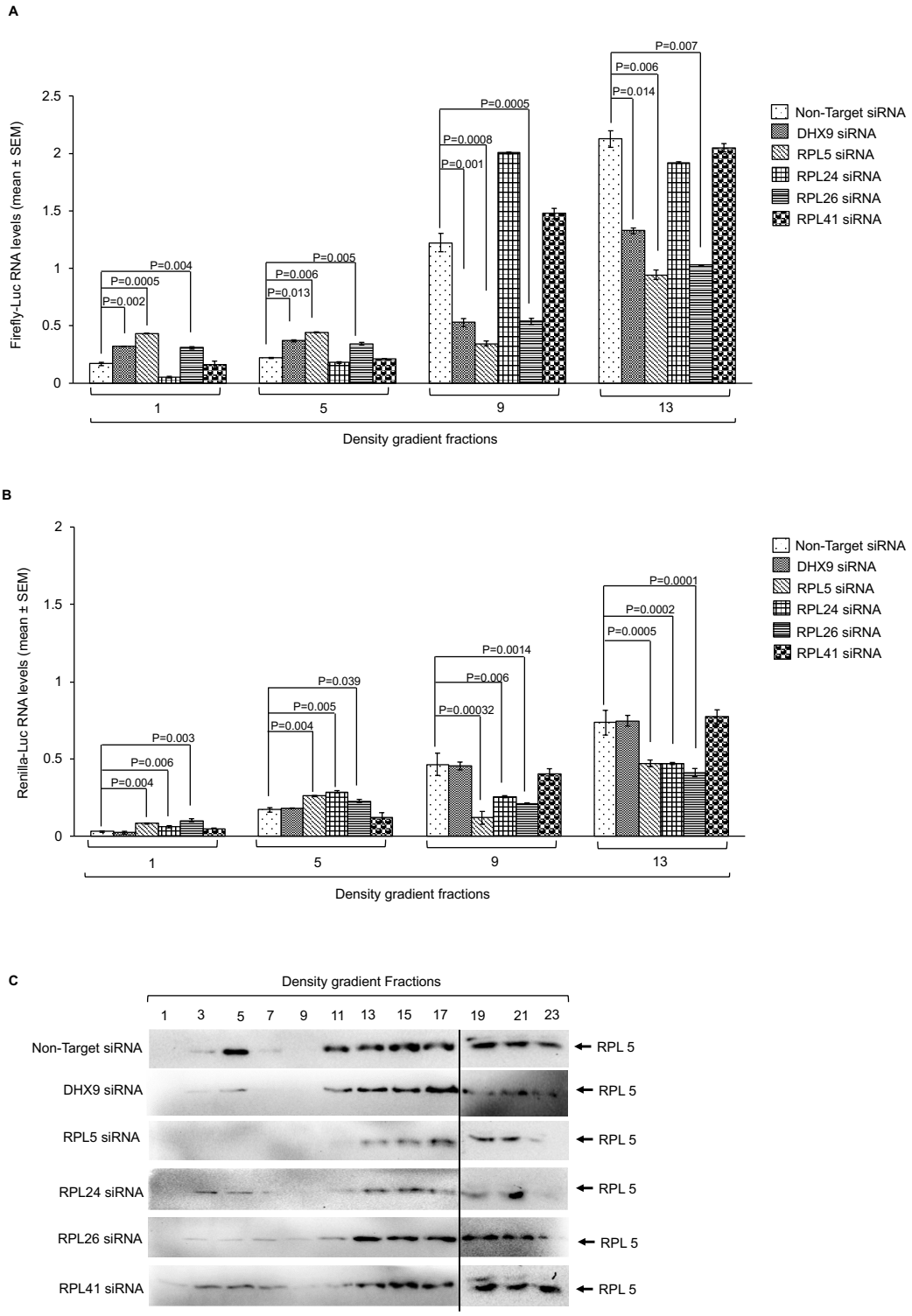

Figure 8. RPL5, RPL26 and RNA helicase A are important for association of the HEV IRESI element with the polysome.

560 (A) RT-qPCR analysis of the Firefly-Luc RNA level in the density gradient fractions 1, 5,
561 9 and 13 of the Huh7 cells, transfected with the indicated siRNAs and the pSuper-HEV
562 IRESl and pRL-TK plasmids for 72 hours and treated with Cycloheximide for 30 minutes.
563 Values are mean (± SEM) of triplicate samples. (B) RT-qPCR analysis of the Renilla-Luc
564 RNA level in the density gradient fractions 1, 5, 9 and 13 of the Huh7 cells, transfected
565 with the indicated siRNAs and the pSuper-HEV IRESl and the pRL-TK plasmids for 72
566 hours and treated with Cycloheximide for 30 minutes. Values are mean (± SEM) of
567 triplicate samples. (C) Western blot analysis of the RPL5 protein level in the indicated
568 density gradient fractions of the Huh7 cells, transfected with the indicated siRNAs and the
569 pSuper-HEV IRESl and the pRL-TK plasmids for 72 hours and treated with Cycloheximide
570 for 30 minutes.

571

572 **Discussion**

573 While investigating the cause of poor replication of the g1-HEV in the Huh7 cells, we
574 observed better viral replication upon treatment of cells with ER stress-inducing
575 compounds such as tunicamycin and thapsigargin. Subsequently, we identified a fourth
576 ORF in the viral genome, which produced the ORF4 protein that played a key role in the
577 assembly of the viral replication complex (32). We also showed that ORF4 was
578 synthesized by an IRES-like (HEV IRESl) element. Sequence analysis of the HEV IRESl
579 indicated its weak homology with the Equine Rhinitis A virus (ERAV) IRES (a type II IRES)
580 (32,46). The HEV IRESl element is remarkably smaller in size than other canonical IRES
581 elements and it requires only 87 nucleotides to drive the cap-independent translation of
582 the ORF4 protein in its native context as well as to drive the translation of a heterologous
583 protein such as the Firefly-Luciferase, when inserted into a bicistronic reporter construct.
584 In contrast, function of known IRES elements depend on double the number of
585 nucleotides or more. Smaller size and relatively simple secondary structure of the HEV
586 IRESl element offers the advantage of dissecting out the molecular mechanisms that are
587 crucial for initiation of cap-independent internal translation. Therefore, the current study
588 was undertaken to further substantiate the claim that HEV IRESl element is a bonafide
589 internal ribosome entry site.

590 Two independent approaches were followed to identify the host interaction partners of the
591 HEV IRESl RNA: RaPID assay and Y3H assay. The RaPID assay identifies stable and
592 transient interactions of all proteins associated with the RNA of interest that includes both
593 direct and indirect interaction partners of the RNA. Several controls were used to
594 avoid/subtract non-specific interaction partners, thus ensuring generation of high
595 confidence mass spectrometry data for downstream studies. For example, good quality
596 of our HEV IRESl RaPID assay-LC-MS-MS data is evident from the fact that comparison
597 of the HEV IRESl-interacting proteins with the SARS-CoV2 5'- and 3'-UTR RNA-
598 interacting proteins (reported by our laboratory using the same technique) identified only
599 RPL7a as the common protein (34). RPL7a is an essential component of the large subunit
600 of ribosome and known to directly bind with RNA through its two distinct RNA binding
601 domains (47). Presence of RPL7a in both the datasets seems to be in agreement with its
602 required function rather than being an experimental artefact.

603 A limitation of the RaPID assay is attributed to its dependence on biotinylation of lysines
604 exposed on the surface of RNA-binding proteins present within 10 nm distance from the
605 BirA ligase. Thus, it is possible to lose some of the RNA binding proteins if they are buried
606 deep inside the complex and inaccessible to BirA ligase for biotinylation. Therefore, a
607 conventional Y3H assay-based human liver cDNA library screening was conducted in
608 parallel to identify the interaction partners of the HEV IRESl RNA. Y3H assay offers the
609 advantage of identifying the direct interaction partners of a bait RNA. Y3H assay identified
610 ribosomal proteins (RPL5, RPL26, RPL41, RPS7, RPS15A and RPS3A), a known DNA
611 binding protein (GREBP) and a cyclophilin family protein (PPIG) as interaction partners
612 of the HEV IRESl (48,45). Specificity of the Y3H data was further ensured by assessing
613 the interaction of the eight HEV IRESl RNA-interacting proteins with two well-known IRES
614 sequences such as the FMDV IRES (Type II IRES) and the HCV IRES (Type IV IRES).
615 Distinct patterns of interaction were observed for these RNA sequences, supporting the
616 specificity of the interactions detected in Y3H assay. Although both RaPID and Y3H
617 assays identified specific interaction partners of HEV IRESl, no common proteins were
618 detected in the two assays. A search of the initial RaPID data of HEV IRESl sample
619 identified RPL26 as a common protein present in both RaPID and Y3H data sets.
620 However, RPL26 was not present in the final list of HEV IRESl interaction partners as it

621 had a PEP score and Prot score of 7 and 29, respectively, whereas the cutoff threshold
622 was set to 17 and 30, respectively. Note that RPL26 was not present in the negative
623 control sample RaPID data.

624 In order to further confirm the interaction between the HEV IRESl RNA and the host
625 proteins, *in vitro* biotinylated-RNA pull down assay and molecular docking analysis was
626 performed for some of the HEV IRESl interacting proteins, which supported their
627 interaction. Docking analysis also demonstrated that the complex between the HEV IRESl
628 and RPL5 was the most stable with respect to the others. Moreover, comparative
629 interaction mapping showed that the interaction of the HEV IRESl element with the
630 ribosomal proteins majorly involved the SL A (nucleotides U9, C10, G12, U22), SL B
631 (nucleotides U29, G30, A38, C41, C44, G50) and the unpaired region between the SL B
632 and SL C (G51, G53, G56, U59, U60, U66, C68) of the former (refer to the HEV IRESl
633 secondary structure in Fig. 1A). In summary, multiple validation steps ensured that the
634 HEV IRESl RNA interaction partners identified in our experiments are of high confidence.

635 Bioinformatics analysis of the 51 HEV IRESl RNA-binding proteins revealed enrichment
636 of proteins involved in the translation process. Eight ribosomal proteins and six translation
637 regulatory factors interact with the HEV IRESl RNA, in support of its function as a
638 translation initiation site**.** Four proteins identified in our study are known to interact with
639 the IRES of other viruses.

640 Silencing of RPL5 significantly inhibited the HEV IRESl activity as well as the g1-HEV
641 replication. RPL5 strongly interacts with the HEV IRESl, weakly interacts with HCV IRES
642 and does not interact with FMDV IRES in Y3H assay. RPL5 showed lowest binding free
643 energy (ΔG) for interaction with the HEV IRESl RNA, *in silico*. RPL5 is also a component
644 of the polysome and lack of RPL5 significantly affected the polysome stability and
645 dissociated both the HEV IRESl and the Renilla-Luc RNAs from the polysome. Hence, it
646 is clear that RPL5 is an essential factor for both cap-dependent and cap-independent
647 translation process. RPL26 showed a pattern similar to RPL5 by inhibiting the HEV IRESl-
648 Luc and Renilla-Luc activities. Moreover, the HEV IRESl-Luc and the Renilla-Luc RNA
649 association with the polysome was significantly reduced upon treatment of cells with the
650 RPL26 siRNA. However, RPL26 differed from RPL5 in the following parameters: it bound

651 moderately with the HEV IRESl RNA both in Y3H assay and *in silico* analysis, lack of
652 RPL26 did not affect g1-HEV replication and lack of RPL 26 did not affect the polysome
653 stability. Earlier studies have shown that lack of RPL26 does not affect cap-dependent
654 translation in *Saccharomyces cerevisiae* and RPL26 is a known ITAF, which has been
655 shown to control DNA damage induced cap-independent translation of the p53 mRNA
656 (49, 50, 51). Based on our data and available literature, we propose that RPL26 may be
657 involved in mediating efficient function of the HEV IRESl though it is not an essential
658 factor. Ablation of both RPL5 and RPL26 may show a more profound effect on the HEV
659 IRESl activity. Further studies are required to clarify the role of RPL26 in mediating the
660 function of HEV IRESl. Silencing of RPL24 and RPL41 did not inhibit either the HEV IRESl
661 activity or the Renilla-Luc activity. Lack of RPL24 reduced the stability of the polysomes,
662 which is in agreement with earlier reports (52). However, lack of RPL24 did not affect the
663 HEV IRESl RNA association with the polysomes although it reduced the association of
664 the Renilla-Luc RNA with the polysomes, indicating its importance in cap-dependent
665 translation. Lack of RPL41 did not affect the polysome stability or HEV IRESl and Renilla
666 RNA association with the polysomes. Interestingly, lack of RPL41 significantly increased
667 the g1-HEV replication, possibly due to extra-translational function of RPL41. Note that
668 RPL41 knockdown has been shown to arrest the cell-cycle in the G2/M phase and it acts
669 by stabilizing the microtubule (53). Our earlier study has shown that HEV replication is
670 significantly high in the G2/M phase of the cell-cycle (54).

671 Apart from the ribosomal proteins, DHX9/RNA helicase A (RHA), HNRNPA2/B1,
672 YTHDF2, EEF2 and LARP4 were also identified as interaction partners of the HEV IRESl
673 RNA. RHA is known to associate with the IRES of FMDV and HCV and acts as an ITAF.
674 It also promotes translation from the IRES of retroviral RNA and jun D mRNA and
675 regulates the replication of several RNA viruses, including the porcine reproductive and
676 respiratory syndrome virus, bovine viral diarrhea virus, classical swine fever virus and
677 dengue virus (55-58). It binds to the 3'-UTR of HEV; however, significance of the
678 interaction is not known (59). RHA is a member of the DEx H-box family of superfamily II
679 (SF2) helicases, which unwind duplex RNA possessing a 3'-single stranded RNA tail by
680 hydrolyzing the nucleoside triphosphates (60, 61). In our experiments, lack of RHA
681 significantly reduced both the HEV IRESl and the Renilla-Luc activities as well as reduced

682 the g1-HEV replication. It was found to be associated with the 40S-80S ribosomes and
683 polysomes, however, its absence did not affect the polysome stability. Lack of RHA
684 resulted in reduced recruitment of the HEV IRESl RNA to the polysomes, however,
685 Renilla-Luc RNA association with the polysomes was not affected. Thus, it is clear that
686 RHA is involved in controlling the activity of the HEV IRESl. HNRNPA2B1 is reported to
687 be involved in mRNA processing. It has been shown to bind to the 3'-UTR of CDK6 and
688 recruit RHA, leading to miRNA mediated silencing of CDK6 (62). An earlier study has
689 shown that HNRNPA2B1 binds to the genomic and sub genomic promoters of HEV and
690 plays an essential role in the g1-HEV replication. Further, intracellular localization of
691 HNRNPA2B1 is altered in the HEV infected cells (63). YTHDF2 is known to accelerate
692 mRNA decay by targeting the mRNAs to cytoplasmic processing bodies (P-bodies) and
693 by recruiting the CCR4-NOT deadenylase complex (64, 65). EEF2 (eukaryotic elongation
694 factor 2) is a GTP binding translation elongation factor, which plays an essential role in
695 translation by promoting GTP dependent translocation of the ribosome (66). LARP4 binds
696 to the poly-A tract of mRNA, associates with the 40S ribosomal subunit as well as
697 polysomes and plays a role in translation regulation by preventing deadenylation at poly-
698 A tail (67-69). Presence of these factors in the HEV IRESl RNA-associated protein
699 complex suggests their potential role(s) in regulating the HEV IRESl-mediated translation.
700 Further studies are warranted to clarify their mode of action.

701 An important aspect of the HEV IRESl function pertains to upregulation of its activity by
702 the ER stress inducing agents in the g1-HEV infected cells (32). The RaPID assay
703 identified four proteins involved in the ER stress response pathway such as the heat
704 shock protein 105 kDa (HSP 105), the luminal ER protein of 29 kDa (ERp29), γ-taxilin and
705 Pumilio homolog 1 (PUM1) as interaction partners of the HEV IRESl. HSP 105 is known
706 to regulate the ER stress induced caspase-3 activation (70). ERP29 is induced by the ER
707 stress. It is ubiquitously expressed and implicated in the biosynthesis and trafficking of
708 many proteins (71). γ-taxilin belongs to the syntaxin-binding protein family, it interacts with
709 ATF4 and regulates the ER stress response (72). PUM1 is known to be phosphorylated
710 by the IRE1 kinase under conditions of ER stress, it binds spliced XBP1 RNA and
711 prevents its degradation (73). Upon ER stress, interaction between PUM1 and HEV IRESl

712 might be protecting the later from degradation by the regulated IRE1-dependent decay
713 (RIDD) pathway.

714 In conclusion, we have identified 51 host proteins, which associate with the HEV IRESl
715 RNA in mammalian cells. Four of the identified proteins have been reported to associate
716 with known IRES elements of viral and cellular origin and two of the identified proteins
717 are known ITAFs. Several ribosomal proteins, translation regulatory factors, components
718 of the tRNA synthetase complex were found to be associated with the HEV IRESl RNA.
719 Taken together, above data unequivocally demonstrate that the HEV IRESl is a bonafide
720 internal ribosome entry site capable of driving cap-independent translation. These
721 findings significantly advance our understanding of the molecular mechanisms that
722 control the synthesis of the ORF4 protein in the g1-HEV infected cells. Moreover,
723 considering the small size and simplicity of the secondary structure of the HEV IRESl
724 element compared to other well-known IRES elements, it is a useful tool for recombinant
725 protein expression as well as for investigating the molecular details of the cap-
726 independent IRES-mediated translation process.

727

728 **Materials and Methods**

729 **Plasmids and reagents**

730 The RNA motif plasmid cloning backbone [(pRMB) (Addgene plasmid # 107253;
731 http://n2t.net/addgene:107253; RRID: Addgene_107253)] and the BASU RaPID plasmid
732 (Addgene plasmid # 107250; http://n2t.net/addgene:107250; RRID:Addgene_107250)
733 were gifted by Prof. Paul A. Khavari (School of Medicine, Stanford University, Clifornia ,
734 USA) and reported earlier (29). To clone the HEV IRESl in the pRMB vector, 2701 to 2787
735 nucleotides of the g1-HEV genome (Genbank ID: AF444002.1) was PCR amplified from
736 the pSK HEV2 plasmid (32) with the following primers: IRESl87 BASU CBB FP (5'
737 GCTTGGTGCCGATCGGTCCC 3') and IRESl87 BASU CBB RP
738 (5'AGCTCATCTGGCAGCAAGCTCAG 3') and ligated with the pRMB vector backbone
739 generated by BSMB1 restriction enzyme digestion, followed by blunting. For hybrid RNA

740 generation for Y3H assay, HEV IRESl, FMDV IRES and HCV IRES sequences were PCR
741 amplified from the pSKHEV2 plasmid, pVitro2-neo-mcs plasmid (InvivoGen, San Diego,
742 USA) and S52/SG-Feo(AI) replicon [gifted by Prof. Charles M. Rice, (74)], respectively,
743 using the following primers: HEV IRESl FP: (5'
744 ACTATCTCGAGGGTGCCGATCGGTCCC 3'), HEV IRESl RP: (5'
745 ACTATCCATGGCATCTGGCAGCAAGCTCAG 3'); FMDV IRES FP: (5'
746 ACTATCTCGAGAGCAGGTTTCCCCAATGACACA 3'), FMDV IRES RP: (5'
747 ACTATCCATGGAAAGGAAAGGTGCCGACCTCCG 3'); HCV IRES FP: (5'
748 ACTATCTCGAGACCTGCCTCTTACGAGGC 3') and HCV IRES RP: (5'
749 ACTATCCATGGTTCTTTGAGGTTTAGGAAGTGTGCT 3'). PCR products were digested
750 with the Xho1 restriction enzyme and ligated with the XhoI and SmaI digested p3HR2
751 vector backbone. To clone the negative sense HEV IRESl (HEVIRESl^{-}) fragment in the
752 p3HR2 vector, 87 nucleotides of IRESl sequence was PCR amplified from the pSK HEV
753 plasmid using HEV IRESl FP and HEV IRESl RP primers and ligated with the SmaI
754 digested p3HR2 vector. To clone the HEV IRESl sequence in the pSuper vector,
755 pRLFF/Luc87 and pSuper plasmids were restriction digested with the BamHI and KpnI
756 enzymes, respectively, followed by treatment with Klenow (end-filled by Klenow) and
757 digestion of both plasmids with XhoI and ligation. To clone the control RNA (618-738 nt
758 in g1-HEV genome) into pGL3 vector (for use in ribosome fractionation assay), pGL3
759 vector was digested with HindIII and NcoI followed by blunting to generate the vector
760 backbone. Next, control RNA sequence was amplified by PCR from pSKHEV2 (Genbank
761 ID: AF444002.1) using Control RNA FP: 5' GCCCCCTGGCACATA 3' and Control RNA
762 RP: 5' GAGCGCAGGTTGGAAA 3'. Linearized pGL3 vector backbone and control RNA
763 sequence insert was ligated and positive clones were selected by restriction digestion.
764 For biotinylated RNA synthesis, HEV IRESl and control RNA sequences were PCR
765 amplified using primers as described above and cloned into pJET1.2 vector, following
766 manufacturer's instruction (Thermo Scientific, Massachusetts, USA). All clones were
767 confirmed by DNA sequencing. All plasmids are available upon request.

768 Human liver cDNA library was obtained from Clontech (California, USA). Dual Luciferase
769 reporter assay kit and CellTiter96 Aqueous one solution cell proliferation assay kits were

770 from Promega (Madison, USA). Non-targeting siRNA (Catalog no. D-001810-10-20),
771 Human RPL5 (6125) siRNA (Catalog no. L-013611-00-0005), Human RPL26 (6154)
772 siRNA (Catalog no. L-011132-01-0005), Human RPL24 (6152) siRNA (Catalog no. L-
773 011144-02-0005), Human RPL41 (6171) siRNA (Catalog no. L-011160-01-0005), Human
774 RPS3A (6188) siRNA (Catalog no. L-013607-00-0005) Human DHX9 (1660) siRNA
775 (Catalog no. L-009950-00-0005) were from Ge Healthcare Dharmacon (Colorado, USA).
776 Antibodies against RPL5 (Catalog no. A303-933A) and RPL26 (Catalog no. A300-686A)
777 were from Bethyl laboratories (Texas, USA). Anti-RPL24 (Catalog No. ITT09128), anti-
778 RPL41 (Catalog No. ITT09136) and anti-DHX9 (Catalog No. ITT12266) antibodies were
779 from Geno Technology Inc. (St Louis, USA); anti-RPS3A (catalog No. STJ28158), anti-
780 RPS7 (catalog No. STJ28814) and anti-PPIG (catalog No. STJ191133) antibodies were
781 from St. John's laboratory (London, UK). Anti-GAPDH (catalog no. sc-25778) antibody
782 was from Santa Cruz Biotechnology (Texas, USA). Goat anti-rabbit IgG-HRP (Cat No.
783 4030-05) was from Southern Biotech (Alabama, USA). 3-Amino 1, 2, 4 triazole (3-AT),
784 Ortho-Nitrophenyl-β-galactoside (ONPG), Cycloheximide and Puromycin was from
785 Sigma (Missouri, USA). Cycloheximide and puromycin were used at a working
786 concentration of 100μg/ml and 0.5μg/ml, respectively.

787 **Mammalian cell-culture, transfection, *in vitro* transcription and cell viability assay**

788 HEK 293T cells were obtained from ATCC (Virginia, USA). Huh7 cells were as described
789 previously (32). Cells were maintained in Dulbecco's modified Eagle medium (DMEM)
790 containing 10% Fetal Bovine Serum (FBS), 50 I.U./mL Penicillin and Streptomycin at
791 37^0C in a 5% CO_2 incubator. Cells were maintained in antibiotic free medium before
792 starting the experiments. For plasmid transfection, cells were seeded at 70-80%
793 confluency in DMEM + 10% FBS and incubated overnight at 37^0C in a 5% CO_2 incubator.
794 Next day, cells were transfected with the desired plasmids using Lipofectamine 2000
795 transfection reagent (Thermo Scientific, Massachusetts, USA), at 1:1 ratio, following
796 manufacturer's instruction. 6-8 hours post-transfection, culture medium was replaced with
797 fresh DMEM+10% FBS.

798 For experiments involving siRNA mediated gene silencing, cells were seeded at 70-80%
799 confluency on 12 well TC dishes and incubated overnight at 37^0C with 5% CO2. Next
800 day, 25nmol siRNA was transfected into each well using 0.35μl Dharmafect transfection
801 reagent, following manufacturer's instruction (GE Healthcare Dharmacon Inc., Colorado,
802 USA). 12 hours post-transfection, culture medium was replaced with fresh medium
803 (DMEM + 10% FBS) and cells were maintained at 37^0C in a 5% CO_2 incubator.

804 The HEV genomic RNA was *in vitro* synthesized as capped RNA, using mMessage
805 mMachine kit (Thermo Scientific, Massachusetts, USA), as described (32). Size and
806 integrity of the *in vitro* synthesized RNA was monitored by formaldehyde agarose gel
807 electrophoresis. *In vitro* synthesized RNA was transfected using Lipofectamine 2000
808 transfection reagent, at 1:1 ratio, following manufacturer's instruction (Thermo Scientific,
809 Massachusetts, USA). 6-8 hours post-transfection, the culture medium was replaced with
810 fresh medium (DMEM+10% FBS) and maintained until further manipulation.

811 For biotinylated-RNA pull down assay, pJET1.2 HEV-IRESl and pJET1.2 Control RNA
812 plasmids were linearized by restriction digestion with NcoI enzyme and column purified.
813 One microgram of purified linearized DNA was used for *in vitro* transcription reaction
814 using Maxi-script T7 transcription kit, following manufacturer's instruction (Thermo
815 Scientific, Massachusetts, USA). 0.2mM Biotin-16-UTP (Sigma-Aldrich,
816 REF:11388908910) and 0.3mM unlabeled-UTP were added to the reaction mixture to
817 produce biotinylated RNA. Non-biotinylated RNAs were transcribed in parallel in the
818 presence of 0.5mM unlabeled UTP. *In vitro* transcribed RNA was purified as per the
819 instruction of the manufacturer of Maxi-script kit.

820 Cell viability was measured using a commercially available kit [CellTiter 96 Aqueous One
821 Solution Cell Proliferation Assay (Promega, Madison, USA)], which utilizes Tetrazolium
822 salt based colorimetric assay. Details are as described (32).

823 **Yeast three Hybrid (Y3H) Assay and screening of the human liver cDNA library**

824 A GAL4 based Y3H assay system, gifted by Prof. Marvin Wickens (University of
825 Wisconsin, Madison, USA) was used to determine the RNA-protein interactions and

826 identification of the HEV IRESl RNA-binding proteins by screening of the human liver
827 cDNA library using the YBZ1 Yeast strain (35).

828 The YBZ1 competent cells were prepared following Lithium Acetate method, as described
829 (75). To examine self-activation by the p3HR2-HEV IRESl, 2µg each of the p3HR2-HEV
830 IRESl and pACT2 plasmids or p3HR2 and pACT2 plasmids were cotransformed into the
831 YBZ1 competent cells and plated on LU^- media, as described (75). After 3 days of
832 incubation in a humidified incubator at 30^0C, 8 random colonies were replica plated onto
833 LUH^- as well as 3-AT (0.1-1 mM) supplemented LUH^- plates, followed by 4 days
834 incubation at 30^0C in a humidified incubator. Colonies were monitored on the 4th day. The
835 p3HR2-HEV IRESl-containing colonies showed very little/no growth on the LUH^- and LUH^-
836 +3-AT media (Figure S2).

837 Next, 2µg of the p3HR2-HEV IRESl plasmid DNA was transformed into the YBZ1
838 competent cells and plated on the U^- media. After 3 days of incubation at 30^0C, a single
839 colony was inoculated in the U^- media and grown at 30^0C to prepare the primary culture
840 (YBZ1-p3HR2-HEV IRESl) and subsequently, the secondary culture. Aliquots of the
841 culture were used for RNA isolation and verification of the HEV-IRESl RNA expression
842 by RT-PCR. Next, the secondary culture grown from the primary culture was used for
843 preparation of competent cells of the YBZ1-p3HR2-HEV IRESl.

844 The human liver Matchmaker cDNA library was procured in the *E.coli BNN132* strain with
845 a titer of $\geq 10^8$ cfu/ml. The cDNA library contained $3.5*10^6$ independent clones, with ~93%
846 colonies containing the cDNA insert. The cDNA library was amplified and a stock titer of
847 $\geq 10^7$ cfu/ml was prepared and stored at -80^0C until further use, following the
848 manufacturer's instruction. Plasmid DNA was isolated from the retitered stock and used
849 for transformation into the YBZ1-p3HR2-HEV IRESl competent cells (YBZ1 strain
850 containing the p3HR2-HEV IRESl plasmid). A pilot transformation was performed to
851 estimate the efficiency of the cDNA library and optimize the ideal quantity of DNA required
852 for screening, following the instructions of the manufacturer. Approximately, $4*10^6$
853 independent library clones were screened on the LUH^- + 0.5mM 3-AT media-containing
854 plates (0.5mM 3-AT was added to enhance the stringency of the screening), leading to

855 growth of 395 colonies. Subsequent replica plating of those 395 colonies on LUH^- plates
856 containing an increasing concentration of 3-AT (2mM, 5mM, 10mM and 20mM) showed
857 that all colonies could grow on 10mM 3-AT or more. These colonies were inoculated in 5
858 ml LU^- media and incubated overnight at 200 RPM, 30^0C, in an incubator-shaker. Next
859 day, cells were harvested by centrifugation at 7000×g, 4^0C, 10 minutes. Plasmid DNA
860 was isolated using the Qiaprep miniprep kit (Qiagen, Hilden, Germany). Briefly, cell pellet
861 was resuspended in the buffer P1 (supplied in the kit), followed by 6 cycles of freeze-thaw
862 in liquid nitrogen and ambient temperature, respectively. Next, the buffer P2 was added,
863 samples were mixed thoroughly and incubated for 5 minutes at ambient temp. Next, buffer
864 N3 was added, samples were mixed thoroughly and centrifuged at 18000×g, 4^0C, 10
865 minutes. Supernatant was loaded onto the kit-supplied columns and plasmid DNA was
866 eluted after a series of washing, as per the instruction of the manufacturer. Plasmid DNA
867 isolated from the YBZ1 transformants were transformed into the *E.coli* Top_{10} strain and
868 colonies were grown on the LB agar media containing ampicillin (100 µg/ml). Presence
869 of the pACT2 plasmid with a cDNA insert sequence in the *E.coli* transformants was
870 verified by a colony PCR using the following primers: pACT2 AD-LT seq FP: (5' ATT
871 CGATGATGAAGATACCCCA 3') and pACT2 AD-LT seq RP: (5'
872 GTGAACTTGCGGGGTTTTTCAGTATCTACGA 3'). 285 colonies were positive in the
873 PCR, indicating that they contained a library clone with a cDNA insert. Plasmid DNA was
874 isolated from these colonies and digested with HindIII, XhoI and EcoRI restriction
875 enzymes to sort them into different categories based on their restriction patterns. 75
876 clones were found to contain unique cDNA insert. The insert and its flanking region was
877 sequenced using the following primer: pACT2 AD LT SEQ Primer:
878 TGGTGGGGTATCTTCATCATCGAATAG. Analysis of the sequencing data identified 8
879 unique protein coding gene sequences in frame with the GAL4 AD. These clones were
880 cotransformed along with the p3HR2-HEV IRESI plasmid into the YBZ1 competent cells
881 with appropriate controls to ensure that the interaction is reproducible and there is no self-
882 activation by the prey protein. Liquid β-galactosidase assay of the colonies were done as
883 described earlier (75).

884 **RaPID assay**

885 The RaPID assay was done as described, following similar conditions (34). To identify
886 the HEV IRESl-interacting host proteins, HEK 293T cells were co-transfected with the
887 pRMB HEV IRESl and BASU plasmids (in 6:1 ratio) using lipofectamine 2000 (1:1 ratio).
888 42 hours post-transfection, 200μM biotin supplemented media (DMEM+10%FBS) was
889 added to the cells and maintained for 18 hours.

890 *Cell lysate preparation:* Cells were washed thrice with ice-cold PBS and lysed in prechilled
891 radio-immunoprecipitation (RIPA) buffer (150 mM NaCl, 1% NP-40, 0.5% sodium
892 deoxycholate, 0.1% SDS, 50mM Tris, pH 8.0), supplemented with protease and
893 phosphatase inhibitor cocktail. The lysate was centrifuged at 14000×g for 40 min and a
894 Macrosep advanced filter (3000 Da MW cutoff, 20 ml; catalogue no. 89131-974; VWR,
895 USA) was used to remove the free biotin. Clarified supernatant was precipitated in
896 acetone, first at -20°C for 10 minutes and then at -80°C for 20 minutes. Protein precipitate
897 was solubilized in 8M urea and Bicinchoninic (BCA) protein assay kit (Thermo Fisher
898 Scientific, MA, USA) was used to determine the protein concentrations of each sample.

899 *Digestion and peptide preparation:* 10mg protein for each sample was treated with 10mM
900 DTT (Dithiothreitol), for 30 min at 56^0C and alkylated with 20mM iodoacetamide (IAA) at
901 room temperature for 1 hour in dark. Trypsin (catalog no. T1426; Thermo Fisher Scientific,
902 MA, USA) was added to the samples at a 1: 20 (wt/wt) ratio and incubated at 37^0C for 24
903 hours. Next, 1% formic acid was added to the samples and desalting of the peptides was
904 done using a Sep-Pak C18 cartridge (catalog no. WAR020515; Waters, MA, USA)
905 followed by lyophilization in a SpeedVac. Lyophilized peptides were solubilized in 1ml
906 PBS and incubated with 150μl pre-washed streptavidin agarose beads (catalog no.
907 20361; Thermo Fisher Scientific, MA, USA) for 2 hours at ambient temperature. The
908 beads were washed in PBS, followed by washing in wash buffer (5% acetonitrile in PBS)
909 and finally with ultrapure water. Excess liquid was completely removed from beads, and
910 biotinylated peptides were eluted by adding 0.3 ml of a solution containing 0.1% formic
911 acid and 80% acetonitrile in water by boiling at 95°C for 5 min. A total of 10 elutions were
912 collected and dried together in a Speed Vac. Enriched peptides were desalted with C18
913 tips (Thermo Fisher Scientific, MA, USA), and reconstituted with solvent A (2%, v/v,
914 acetonitrile, 0.1% v/v, formic acid in water) for LC-MS/MS analysis.

915 *LC-MS/MS acquisition:* A Sciex 5600^{+} triple time of flight (TOF) mass spectrometer was
916 used for LC-MS/MS analysis. It was coupled with a chromXP reversed-phase 3-µm C_{18}-
917 CL trap column (350 µm by 0.5 mm, 120 Å; Eksigent; AB Sciex, MA, USA) and a
918 nanoViper C_{18} separation column (75 µm by 250 mm, 3 µm, 100 Å; Acclaim PepMap;
919 Thermo Fisher Scientific, MA, USA) in an Eksigent nanoLC (ultra 2D plus) system. A
920 binary mobile solvent system was applied, with the following composition: solvent C, 2%
921 (v/v) acetonitrile, 0.1% (v/v) formic acid in water; solvent B, 98% (v/v) acetonitrile, 0.1%
922 (v/v) formic acid. To separate the peptides, a 60 minutes gradient was run with a total run
923 time of 90 minutes at a flow rate of 200 nl/minute and MS data was acquired in information
924 dependent-acquisition (IDA) with high sensitivity mode. Each cycle was run for 2.3
925 seconds with 250- and 100-ms acquisition times for MS1 (*m/z* 350 to 1,250 Da) and
926 MS/MS (100 to 1,800 *m/z*) scans, respectively. Every experimental condition was run in
927 quadruplets.

928 *Protein identification and quantification:* All raw files (.wiff) were searched in protein Pilot
929 software (version 4.5; Sciex) with Mascot algorithm for protein identification and semi
930 quantitation against Swiss-Prot_57.15 database (20,266 sequences after application of
931 *Homo sapiens* taxonomy filter). Following parameters were applied to search biotinylated
932 peptides: (a) Trypsin as a proteolytic enzyme with maximum of two missed cleavages
933 allowed; (b) Allowed tolerance limit for peptide mass error was 20ppm;(c) Mass error
934 tolerance for fragments was taken up to 0.20 Da; (d) Carbamido-methylation of cysteine
935 (+ 57.02146 Da), oxidation of methionine (+15.99491 Da), deamination of NQ (+
936 0.98416), and biotinylation of lysine (+ 226.07759 Da) were taken as variable
937 modifications. Pearson correlation plot of peptide intensity was used to monitor the quality
938 of data between each run and replicates.

939 *Data analysis:* A protein was considered to be identified if it corresponds to one or more
940 biotinylated peptide, with PEP (posterior error probability) score ≥ the median value in the
941 Gaussian smoothing curve of each sample. Note that PEP score refers to the probability
942 that the observed peptide spectrum matches are incorrect. A web-based tool,
943 Bioinformatics and Evolutionary Genomics (http://bioinformatics.psb.ugent.be/
944 webtools/Venn/) was used to identify host proteins that are specific to HEV IRESI RNA

945 and formation of Venn diagram. Data set with a minimum of 1 unique peptide and a "prot
946 score" of 30 or more was considered in the final list of host proteins for further studies
947 (Table1). "Prot Score" refers to the overall protein score generated by Mascot,
948 considering all the observed mass spectrums, which match amino acid sequences of a
949 certain protein.

950 *Data availability:* The mass spectrometry proteomics data have been deposited to the
951 ProteomeXchange Consortium via the PRIDE partner repository with the dataset identifier
952 PXD031009.

953 **Bioinformatics analysis**

954 RNA secondary structures were analyzed using the Mfold program
955 (http://www.unafold.org/mfold/applications/rna-folding-form.php), based on a minimum
956 free energy calculation at 25^0C (76). The host-virus RPPI data set was visualized using
957 Cytoscape (version 3.1.0). Network Analyzer plug-in in Cytoscape was used to compute
958 the topological parameters and centrality measures of the network. Gene ontology (GO)
959 and Reactome pathway analysis were performed using the Gene Set Enrichment
960 (https://www.gseamsigdb.org/gsea/index.jsp) and Enrichr
961 (https://maayanlab.cloud/Enrichr) (77) tools.

962 ***In silico* analysis of the RNA-protein interactions**

963 The protein structures of the four targets RPS3A, RPS7, RPL5, RPL26 are not reported,
964 therefore, their sequences were retrieved from the "uniport" by using their id numbers
965 P61247, P62081, P46777, and P61254, respectively. Furthermore, the i-tasser module
966 was used to build their 3D structures. Based on their c-score, the best model was selected
967 and evaluated through Ramachandran plots. Furthermore, the energy minimization of
968 each protein was carried out using AMBER tool. The 3dRNA tool is used to generate the
969 3D of RNA sequence. For Protein-RNA docking, the HDOCK was used with the standard
970 cut-offs. In each docking the top complex was picked for further analysis. The energy
971 minimized complex structures were used for their quantitative and thermodynamic
972 analysis.

973 **Luciferase reporter assay, Western blot analysis, RNA isolation and quantitative**
974 **real time PCR (RTq-PCR)**

975 To perform the dual luciferase reporter assay, the HEK 293T cells were seeded at 70%
976 confluency and next day, 25nM siRNA were transfected in respective wells using 0.35µl
977 of Dharmafect transfection reagent as per manufacturer's instructions (GE Healthcare
978 Dharmacon Inc. Co, USA). 12 hours post transfection of siRNA, media was changed
979 followed by transfection of the dual luciferase reporter plasmids (pRLFF/luc87, 1µg/well)
980 using lipofectamine 2000 at 1:1 (wt/v) ratio. 8 hours later, media was changed and cells
981 were incubated for 48 hours. Cells were washed with ice cold PBS and used for
982 luciferase assay using the dual glow Luciferase assay kit, following manufacturer's
983 protocol (Promega, Wisconsin, USA). The Firefly-Luc values were divided by that of the
984 Renilla-Luc or divided by the percentage cell-viability, as specified in the results and
985 graphs were plotted in GraphPad prism or Microsoft Excel. Values are mean (± SEM) of
986 three independent experiments done in triplicates. Western blot was done as described
987 (32). Total cellular RNA was isolated using the TRI reagent (MRC Inc., Cincinnati, USA)
988 as per manufacturer's protocol. cDNA was synthesized using random hexamers and a
989 commercial cDNA synthesis kit, following manufacturer's protocol (Firescript cDNA
990 synthesis kit, Solis BioDyne, Tartu, Estonia). RTq-PCR was done by SYBR green
991 detection method using a commercially available kit (5X Hot Firepol Evagreen qPCR
992 mix plus, Solis BioDyne, Tartu, Estonia). Following primers were used to detect the
993 levels of g1-HEV RNA, HEV IRESl RNA, Renilla-Luc RNA and control RNA (618-738 nt
994 in g1-HEV genome): g1-HEV FP: (5' CGGCCCAGTCTATGTCTCTG 3'), g1-HEV RP:
995 (TAGTTCCTGCCTCCCAAAAG 3'); HEV IRESl FP (5'
996 TATACTCGAGGGTGCCGATCGGTCCC 3'), HEV IRESl RP (5'
997 TATACCATGGCATCTGGCAGCAAGCTCAG 3'); R-Luc FP (5'
998 CTTCTTATTTATGGCGACATGTT 3') and R-Luc RP (5' GCCTGATTTGCCCATACC
999 AATA 3'); Control RNA FP (5' GCCCCCTGGCACATA 3') and Control RNA RP (5'
1000 GAGCGCAGGTTGGAAA 3').

1001

1002 **Ribosome fractionation assay**

1003 Ribosome fractionation was done as described (43, 44). HEK 293T cells were seeded at
1004 70% confluency in 100 mm dishes and transfected with the pGL3-control RNA, pSuper-
1005 HEV IRESl and pRL-TK plasmid DNA (12µg/dish) using lipofectamine 2000 (1:1 ratio).
1006 48 hours post-transfection, 100 µg/ml of cycloheximide (CHX) or 0.5µg/ml of puromycin
1007 (Puro) was added to the culture medium and incubation was continued for 30 minutes at
1008 37^0C, with 5% CO_2. Next, cells were washed three times with ice cold PBS (containing
1009 100 µg/ml CHX, in case of CHX treatment) followed by trypsinization and centrifugation
1010 for 5 minutes at 500×g. Supernatant was discarded and the cell pellet was resuspended
1011 in 1ml polysome extraction buffer (PEB, 20mM Tris-HCl, pH 7.5, 100mM KCl, 5mM $MgCl_2$,
1012 0.5% Nonidet P-40, 100µg/ml CHX, 1X protease inhibitors and 1:1000 dilution of
1013 RiboLock RNase inhibitor), incubated on ice for 30 minutes with occasional mixing,
1014 centrifuged at 12000×g for 20 minutes at 4^0C. Total protein and RNA concentration in the
1015 clarified lysate was measured by Bradford assay or Nanodrop spectrophotometry,
1016 respectively. Aliquots of the lysate were used for cDNA synthesis, western blot analysis
1017 and ribosome fractionation.

1018 A linear 10% - 50% sucrose density gradient was prepared for ribosome fractionation,
1019 one day before the polysome fractionation experiment. Stock solutions of 10%, 20%,
1020 30%, 40% and 50% sucrose were prepared using 2.2M sucrose and 10x salt solution
1021 (1000 mM NaCl, 200mM Tris-HCl, pH 7.5, 50 mM $MgCl_2$) in Diethyl Pyrocarbonate
1022 (DEPC)-treated water. 2.2 ml of 10% stock solution of sucrose was added to the bottom
1023 of a thin-wall 12.5 ml ultracentrifuge tube, followed by addition of 2.2 ml each of 20%,
1024 30%, 40%, and 50% sucrose solutions. Tubes were stored at 4^0C, overnight for
1025 linearization. Next day, equal amount of clarified lysate was loaded to the top of the tubes
1026 and weights were equalized. Tubes were run in a SW40Ti swinging bucket rotor at
1027 190000×g for 90 minutes at 4^0C, using a Beckman ultracentrifuge (Beckman Coulter,
1028 California, USA). After centrifugation, tubes were set for fractionation in the automated
1029 fraction collection unit and 24 fractions of 500 µl each were collected. Profile of RNA in
1030 the fractions was captured as an indicator of different ribosome fractions (shown in Fig.

1031 S4A). Alternate fractions (1-23) were selected for further analysis of RNA and protein
1032 distribution profiles.

1033 **M^7G capped-RNA and biotinylated-RNA pull down assay**

1034 For m^7G capped RNA pulldown, HEK 293T cells were seeded in 60 mm dishes at a
1035 confluency of 70%. Next day, cells were cotransfected with 2µg each of the pSuper-HEV
1036 IRESl and pRL-TK plasmids and cells were incubated for 48 hours in DMEM media
1037 supplemented with 10% FBS in a 37^0C incubator supplied with 5% CO_2. Next, cells were
1038 lysed in 1ml TRI reagent and RNA was extracted as per manufacturer's instructions (MRC
1039 Inc, Cincinnati, USA). 20µg of total RNA was added to the binding buffer [1% Triton X-
1040 100, 150mM NaCl, 2mM EDTA (pH 8.0), 20mM Tris-HCl (pH 8.0)], 20 µl monoclonal anti-
1041 m^7G cap antibody (Merck, Massachusetts, USA) and 1µl RNAse inhibitor (RNAsin,
1042 Promega, Wisconsin, USA) was added to that and samples were incubated overnight at
1043 4°C with continuous mixing. 25 µl Protein G-PLUS-Agarose beads (Santa Cruz
1044 Biotechnology, Santacruz, USA) were washed twice in the binding buffer and added to
1045 the samples, followed by one hour incubation. Samples were centrifuged at 1000 rpm for
1046 1 minute at 4^0C. Supernatant containing unbound RNA was collected, RNA was extracted
1047 using TRI reagent and stored at -80^0C. Beads were washed four times in ice cold low salt
1048 wash buffer [1% SDS, 1% Triton X-100, 150mM NaCl, 2mM EDTA (pH 8.0), 20mM Tris-
1049 HCl (pH 8.0)] and once in high salt wash buffer [1% SDS, 1% Triton X-100, 500mM NaCl,
1050 2mM EDTA (pH 8.0) 20mM Tris-HCl (pH 8.0)] and twice with Tris-EDTA buffer (pH 8.0).
1051 Finally, beads were re-suspended in the elution buffer (1% SDS, 0.1M NaHCO3),
1052 incubated for 5 minutes at 4^0C on a rocker, followed by centrifugation at 1000 rpm for 1
1053 minute at 4^0C and collection of the supernatant. RNA was isolated from the supernatant
1054 using TRI reagent and all samples were simultaneously processed for RT-qPCR.

1055 For biotinylated RNA pulldown assay, 10^7 Huh7 cells were lysed in the binding buffer [1%
1056 Triton X-100, 0.5% NP-40, 150mM NaCl, 2mM EDTA (pH 8.0), 20mM Tris-HCl (pH 8.0),
1057 1X complete protease inhibitor cocktail, 40 units RNAse inhibitor] and clarified lysate were
1058 incubated with biotinylated control RNA [control RNA (B^+)], non-biotinylated HEV IRESl
1059 RNA [HEV IRESl RNA (B^-)], biotinylated HEV IRESl RNA [HEV IRESl RNA (B^+)] or mock

1060 lysate (Cell lysate without RNA) for 1 hour on a flip-flop rocker at 4^0C. Streptavidin
1061 magnetic beads were washed twice in binding buffer and added to the RNA-protein
1062 mixture, followed by incubation for 1 hour, under similar condition. Streptavidin bound
1063 RNA-protein complex were washed two times in ice cold low salt wash buffer [1% SDS,
1064 1% Triton X-100, 150mM NaCl, 2mM EDTA (pH 8.0), 20mM Tris-HCl (pH 8.0)] and once
1065 in high salt wash buffer [1% SDS, 1% Triton X-100, 250mM NaCl, 2mM EDTA (pH 8.0)
1066 20mM Tris-HCl (pH 8.0)] and once with Tris-EDTA buffer (pH 8.0). 50% of the beads were
1067 re-suspended in the elution buffer (1% SDS, 0.1M $NaHCO_3$), incubated for 5 minutes at
1068 4^0C on a rocker, followed by collection of the supernatant for checking the presence of
1069 RNA by formaldehyde-agarose gel electrophoresis. Rest of the beads were mixed with
1070 2X Laemmli buffer, incubated at 95^0C for 5 minutes, followed by collection of the
1071 supernatant for western blot analysis using various antibodies.

1072 **Statistical analysis**

1073 Data are shown as mean ± standard error of mean (SEM) of three independent
1074 experiments. *P*-values were calculated by two tailed Student t-test (paired two samples
1075 for means).

1076 **Acknowledgments**

1077 RNA motif plasmid cloning backbone (pRMB) and BASU RaPID plasmid were kindly
1078 gifted by Prof. Paul Khavari. We thank Prof. Marvin Wickens for providing the Y3H assay
1079 system. We thank Prof Charles M. Rice for providing the g3A HCV replicon. We thank
1080 Mr. Dipanka Tanu Sarmah and Dr. Samrat Chatterjee for data analysis using “Enrich R”.
1081 We thank Dr. Saumya Anang and Dr. Chandru Subramani for helping in the initial
1082 experiments. We appreciate continuous support by the technical staff of RCB mass
1083 spectrometry facility in data collection. This study was funded by the Science and
1084 Engineering Research Board (SERB), Govt of India, grant to MS and THSTI core grant
1085 to MS. SK is supported by a senior research fellowship from the Department of
1086 Biotechnology, Govt of India, RV and SS are supported by a senior research fellowship
1087 from the Council of Scientific and Industrial Research, Govt of India.

1088

1089 **References**

1090 1. Merrick WC, Pavitt GD. Protein synthesis initiation in eukaryotic cells. Cold Spring
1091 Harbor perspectives in biology. 2018;10(12): a033092.
1092 2. Shatsky IN, Terenin IM, Smirnova VV, Andreev DE. Cap-independent translation:
1093 what's in a name?. Trends in biochemical sciences. 2018;43(11):882-95.
1094 3. Shatsky IN, Dmitriev SE, Terenin IM, Andreev DE. Cap-and IRES-independent
1095 scanning mechanism of translation initiation as an alternative to the concept of
1096 cellular IRESs. Molecules and cells. 2010 ;30(4):285-93.
1097 4. Kaiser C, Dobrikova EY, Bradrick SS, Shveygert M, Herbert JT, Gromeier M.
1098 Activation of cap-independent translation by variant eukaryotic initiation factor 4G in
1099 vivo. RNA. 2008;14(10):2170-82.
1100 5. Trainor BM, Ghosh A, Pestov DG, Hellen CU, Shcherbik N. A translation enhancer
1101 element from black beetle virus engages yeast eIF4G1 to drive cap-independent
1102 translation initiation. Scientific reports. 2021;11(1):1-8.
1103 6. Meyer KD, Patil DP, Zhou J, Zinoviev A, Skabkin MA, Elemento O, Pestova TV, Qian
1104 SB, Jaffrey SR. 5′ UTR m6A promotes cap-independent translation. Cell.
1105 2015;163(4):999-1010.
1106 7. Meyer KD, Saletore Y, Zumbo P, Elemento O, Mason CE, Jaffrey SR.
1107 Comprehensive analysis of mRNA methylation reveals enrichment in 3′ UTRs and
1108 near stop codons. Cell. 2012;149(7):1635-46.
1109 8. Wang X, Zhao BS, Roundtree IA, Lu Z, Han D, Ma H, Weng X, Chen K, Shi H, He C.
1110 N6-methyladenosine modulates messenger RNA translation efficiency. Cell.
1111 2015;161(6):1388-99.
1112 9. Lee KM, Chen CJ, Shih SR. Regulation mechanisms of viral IRES-driven translation.
1113 Trends in microbiology. 2017;25(7):546-61.
1114 10. Brown EA, Zajac AJ, Lemon SM. In vitro characterization of an internal ribosomal
1115 entry site (IRES) present within the 5'nontranslated region of hepatitis A virus RNA:
1116 comparison with the IRES of encephalomyocarditis virus. Journal of virology.
1117 1994;68(2):1066-74.
1118 11. Ali IK, McKendrick L, Morley SJ, Jackson RJ. Activity of the hepatitis A virus IRES
1119 requires association between the cap-binding translation initiation factor (eIF4E) and
1120 eIF4G. Journal of virology. 2001;75(17):7854-63.
1121 12. Kerr CH, Jan E. Commandeering the ribosome: Lessons learned from dicistroviruses
1122 about translation. Journal of virology. 2016;90(12):5538-40.
1123 13. Khawaja A, Vopalensky V, Pospisek M. Understanding the potential of hepatitis C
1124 virus internal ribosome entry site domains to modulate translation initiation via their
1125 structure and function. Wiley Interdisciplinary Reviews: RNA. 2015;6(2):211-24.

1126 14. Pestova TV, Hellen CU. Translation elongation after assembly of ribosomes on the
1127 Cricket paralysis virus internal ribosomal entry site without initiation factors or initiator
1128 tRNA. Genes & development. 2003;17(2):181-6.
1129 15. Wilson JE, Pestova TV, Hellen CU, Sarnow P. Initiation of protein synthesis from the
1130 A site of the ribosome. Cell. 2000;102(4):511-20.
1131 16. Song Y, Mugavero J, Stauft CB, Wimmer E. Dengue and Zika virus 5′ untranslated
1132 regions harbor internal ribosomal entry site functions. MBio. 2019;10(2):e00459-19.
1133 17. Fernández-García L, Angulo J, Ramos H, Barrera A, Pino K, Vera-Otarola J, López-
1134 Lastra M. The Internal Ribosome Entry Site of Dengue Virus mRNA Is Active When
1135 Cap-Dependent Translation Initiation Is Inhibited. Journal of virology.
1136 2020;95(5):e01998-20.
1137 18. Edgil D, Polacek C, Harris E. Dengue virus utilizes a novel strategy for translation
1138 initiation when cap-dependent translation is inhibited. Journal of virology.
1139 2006;80(6):2976-86.
1140 19. Brasey A, Lopez-Lastra M, Ohlmann T, Beerens N, Berkhout B, Darlix JL, Sonenberg
1141 N. The leader of human immunodeficiency virus type 1 genomic RNA harbors an
1142 internal ribosome entry segment that is active during the G2/M phase of the cell cycle.
1143 Journal of virology. 2003;77(7):3939-49.
1144 20. Vallejos M, Deforges J, Plank TD, Letelier A, Ramdohr P, Abraham CG, Valiente-
1145 Echeverría F, Kieft JS, Sargueil B, Lopez-Lastra M. Activity of the human
1146 immunodeficiency virus type 1 cell cycle-dependent internal ribosomal entry site is
1147 modulated by IRES trans-acting factors. Nucleic acids research. 2011;39(14):6186-
1148 200.
1149 21. Ohlmann T, Lopez-Lastra M, Darlix JL. An internal ribosome entry segment promotes
1150 translation of the simian immunodeficiency virus genomic RNA. Journal of Biological
1151 Chemistry. 2000;275(16):11899-906.
1152 22. Barrera A, Olguín V, Vera-Otarola J, López-Lastra M. Cap-independent translation
1153 initiation of the unspliced RNA of retroviruses. Biochimica et Biophysica Acta (BBA)-
1154 Gene Regulatory Mechanisms. 2020;1863(9):194583.
1155 23. Shi B, Song Q, Luo X, Song J, Xia D, Xia Z, Liu M, Wang W, Wang R, Du H, Han J.
1156 Identification of cryptic putative IRESs within the ORF encoding the nonstructural
1157 proteins of the human rhinovirus 16 genome. Archives of virology.
1158 2021;166(12):3373-86.
1159 24. Shi B, Song Q, Luo X, Song J, Xia D, Xia Z, Liu M, Wang W, Wang R, Du H, Wei Q.
1160 Identification of an IRES within the coding region of the structural protein of human
1161 rhinovirus 16. Journal of Medical Virology. 2021.
1162 25. Grainger L, Cicchini L, Rak M, Petrucelli A, Fitzgerald KD, Semler BL, Goodrum F.
1163 Stress-inducible alternative translation initiation of human cytomegalovirus latency
1164 protein pUL138. Journal of virology. 2010;84(18):9472-86.

1165 26. May J, Johnson P, Saleem H, Simon AE. A sequence-independent, unstructured
1166 internal ribosome entry site is responsible for internal expression of the coat protein
1167 of Turnip crinkle virus. Journal of Virology. 2017;91(8):e02421-16.
1168 27. Nimgaonkar I, Ding Q, Schwartz RE, Ploss A. Hepatitis E virus: advances and
1169 challenges. Nature Reviews Gastroenterology & Hepatology. 2018;15(2):96-110.
1170 28. Surjit M, Liu B, Chow VT, Lal SK. The nucleocapsid protein of severe acute
1171 respiratory syndrome-coronavirus inhibits the activity of cyclin-cyclin-dependent
1172 kinase complex and blocks S phase progression in mammalian cells. Journal of
1173 Biological Chemistry. 2006;281(16):10669-81.
1174 29. Nagashima S, Takahashi M, Tanaka T, Yamada K, Nishizawa T, Okamoto H. A PSAP
1175 motif in the ORF3 protein of hepatitis E virus is necessary for virion release from
1176 infected cells. Journal of general virology. 2011;92(2):269-78.
1177 30. Ding Q, Heller B, Capuccino JM, Song B, Nimgaonkar I, Hrebikova G, Contreras JE,
1178 Ploss A. Hepatitis E virus ORF3 is a functional ion channel required for release of
1179 infectious particles. Proceedings of the National Academy of Sciences.
1180 2017;114(5):1147-52.
1181 31. Xu LD, Zhang F, Peng L, Luo WT, Chen C, Xu P, Huang YW. Stable expression of a
1182 hepatitis E Virus (HEV) RNA replicon in two mammalian cell lines to assess
1183 mechanism of innate immunity and antiviral response. Frontiers in microbiology.
1184 2020:3093.
1185 32. Nair VP, Anang S, Subramani C, Madhvi A, Bakshi K, Srivastava A, Nayak B, CT RK,
1186 Surjit M. Endoplasmic reticulum stress induced synthesis of a novel viral factor
1187 mediates efficient replication of genotype-1 hepatitis E virus. PLoS pathogens.
1188 2016;12(4):e1005521.
1189 33. Ramanathan M, Majzoub K, Rao DS, Neela PH, Zarnegar BJ, Mondal S, Roth JG,
1190 Gai H, Kovalski JR, Siprashvili Z, Palmer TD. RNA–protein interaction detection in
1191 living cells. Nature methods. 2018;15(3):207-12.
1192 34. Verma R, Saha S, Kumar S, Mani S, Maiti TK, Surjit M. RNA-Protein Interaction
1193 Analysis of SARS-CoV-2 5′ and 3′ Untranslated Regions Reveals a Role of
1194 Lysosome-Associated Membrane Protein-2a during Viral Infection. mSystems.
1195 2021;6(4):e00643-21.
1196 35. Koh YY, Wickens M. Determining the RNA specificity and targets of RNA-binding
1197 proteins using a three-hybrid system. Methods in enzymology. 2014; (Vol. 539:163-
1198 181). Academic Press.
1199 36. Cho SK, Kang IH, Carr T, Hannapel DJ. Using the yeast three-hybrid system to
1200 identify proteins that interact with a phloem-mobile mRNA. Frontiers in Plant Science.
1201 2012;3:189.
1202 37. Pacheco A, Reigadas S, Martínez-Salas E. Riboproteomic analysis of polypeptides
1203 interacting with the internal ribosome-entry site element of foot-and-mouth disease
1204 viral RNA. Proteomics. 2008;8(22):4782-90.

38. Otto GA, Lukavsky PJ, Lancaster AM, Sarnow P, Puglisi JD. Ribosomal proteins mediate the hepatitis C virus IRES–HeLa 40S interaction. RNA. 2002;8(7):913-23.
39. Godet AC, David F, Hantelys F, Tatin F, Lacazette E, Garmy-Susini B, Prats AC. IRES trans-acting factors, key actors of the stress response. International Journal of Molecular Sciences. 2019;20(4):924.
40. Kappel K, Jarmoskaite I, Vaidyanathan PP, Greenleaf WJ, Herschlag D, Das R. Blind tests of RNA–protein binding affinity prediction. Proceedings of the National Academy of Sciences. 2019;116(17):8336-41.
41. Yan Y, Zhang D, Zhou P, Li B, Huang SY. HDOCK: a web server for protein–protein and protein–DNA/RNA docking based on a hybrid strategy. Nucleic acids research. 2017;45(W1):W365-73.
42. Jia D, Cai L, He H, Skogerb G, Li T, Aftab MN, Chen R. Systematic identification of non-coding RNA 2, 2, 7-trimethylguanosine cap structures in Caenorhabditis elegans. BMC molecular biology. 2007;8(1):1-9.
43. Panda AC, Martindale JL, Gorospe M. Polysome fractionation to analyze mRNA distribution profiles. Bio-protocol. 2017;7(3).
44. Chassé H, Boulben S, Costache V, Cormier P, Morales J. Analysis of translation using polysome profiling. Nucleic acids research. 2017;45(3):e15-e15.
45. Davis TL, Walker JR, Campagna-Slater V, Finerty Jr PJ, Paramanathan R, Bernstein G, MacKenzie F, Tempel W, Ouyang H, Lee WH, Eisenmesser EZ. Structural and biochemical characterization of the human cyclophilin family of peptidyl-prolyl isomerases. PLoS biology. 2010;8(7):e1000439.
46. Hinton TM, Li F, Crabb BS. Internal ribosomal entry site-mediated translation initiation in equine rhinitis A virus: similarities to and differences from that of foot-and-mouth disease virus. Journal of Virology. 2000;74(24):11708-16.
47. Russo G, Cuccurese M, Monti G, Russo A, Amoresano A, Pucci P, Pietropaolo C. Ribosomal protein L7a binds RNA through two distinct RNA-binding domains. Biochemical Journal. 2005;385(1):289-99.
48. Martel G, Hamet P, Tremblay J. GREBP, a cGMP-response element-binding protein repressing the transcription of natriuretic peptide receptor 1 (NPR1/GCA). Journal of Biological Chemistry. 2010;285(27):20926-39.
49. Babiano R, Gamalinda M, Woolford Jr JL, de la Cruz J. Saccharomyces cerevisiae ribosomal protein L26 is not essential for ribosome assembly and function. Molecular and cellular biology. 2012;32(16):3228-41.
50. Chen J, Guo K, Kastan MB. Interactions of nucleolin and ribosomal protein L26 (RPL26) in translational control of human p53 mRNA. Journal of Biological Chemistry. 2012;287(20):16467-76.
51. Takagi M, Absalon MJ, McLure KG, Kastan MB. Regulation of p53 translation and induction after DNA damage by ribosomal protein L26 and nucleolin. Cell. 2005;123(1):49-63.

1245 52. Wilson-Edell KA, Kehasse A, Scott GK, Yau C, Rothschild DE, Schilling B, Gabriel
1246 BS, Yevtushenko MA, Hanson IM, Held JM, Gibson BW. RPL24: a potential
1247 therapeutic target whose depletion or acetylation inhibits polysome assembly and
1248 cancer cell growth. Oncotarget. 2014;5(13):5165.
1249 53. Wang S, Huang J, He J, Wang A, Xu S, Huang SF, Xiao S. RPL41, a small ribosomal
1250 peptide deregulated in tumors, is essential for mitosis and centrosome integrity.
1251 Neoplasia. 2010;12(3):284-IN8.
1252 54. Subramani C, Nair VP, Anang S, Mandal SD, Pareek M, Kaushik N, Srivastava A,
1253 Saha S, Shalimar, Nayak B, Ranjith-Kumar CT. Host-virus protein interaction network
1254 reveals the involvement of multiple host processes in the life cycle of hepatitis E virus.
1255 MSystems. 2018;3(1):e00135-17.
1256 55. Hartman TR, Qian S, Bolinger C, Fernandez S, Schoenberg DR, Boris-Lawrie K. RNA
1257 helicase A is necessary for translation of selected messenger RNAs. Nature structural
1258 & molecular biology. 2006;13(6):509-16.
1259 56. Bolinger C, Sharma A, Singh D, Yu L, Boris-Lawrie K. RNA helicase A modulates
1260 translation of HIV-1 and infectivity of progeny virions. Nucleic acids research.
1261 2010;38(5):1686-96.
1262 57. Bolinger C, Yilmaz A, Hartman TR, Kovacic MB, Fernandez S, Ye J, Forget M, Green
1263 PL, Boris-Lawrie K. RNA helicase A interacts with divergent lymphotropic retroviruses
1264 and promotes translation of human T-cell leukemia virus type 1. Nucleic acids
1265 research. 2007;35(8):2629-42.
1266 58. Shi RZ, Pan YQ, Xing L. RNA Helicase A Regulates the Replication of RNA Viruses.
1267 Viruses. 2021;13(3):361.
1268 59. Paingankar MS, Arankalle VA. Identification and characterization of cellular proteins
1269 interacting with Hepatitis E virus untranslated regions. Virus research. 2015;208:98-
1270 109.
1271 60. Koh HR, Xing L, Kleiman L, Myong S. Repetitive RNA unwinding by RNA helicase A
1272 facilitates RNA annealing. Nucleic acids research. 2014;42(13):8556-64.
1273 61. Zhang S, Grosse F. Domain structure of human nuclear DNA helicase II (RNA
1274 helicase A). Journal of Biological Chemistry. 1997;272(17):11487-94.
1275 62. Yin M, Cheng M, Liu C, Wu K, Xiong W, Fang J, Li Y, Zhang B. HNRNPA2B1 as a
1276 trigger of RNA switch modulates the miRNA-mediated regulation of CDK6. Iscience.
1277 2021;24(11):103345.
1278 63. Pingale KD, Kanade GD, Karpe YA. Heterogeneous Nuclear Ribonucleoproteins
1279 Participate in Hepatitis E Virus Replication. Journal of Molecular Biology. 2020 Mar
1280 27;432(7):2369-87.
1281 64. Wang X, Lu Z, Gomez A, Hon GC, Yue Y, Han D, Fu Y, Parisien M, Dai Q, Jia G,
1282 Ren B. N6-methyladenosine-dependent regulation of messenger RNA stability.
1283 Nature. 2014;505(7481):117-20.

1284 65. Du H, Zhao Y, He J, Zhang Y, Xi H, Liu M, Ma J, Wu L. YTHDF2 destabilizes m6A-
1285 containing RNA through direct recruitment of the CCR4–NOT deadenylase complex.
1286 Nature communications. 2016;7(1):1-1.
1287 66. Kaul G, Pattan G, Rafeequi T. Eukaryotic elongation factor-2 (eEF2): its regulation
1288 and peptide chain elongation. Cell biochemistry and function. 2011;29(3):227-34.
1289 67. Mattijssen S, Arimbasseri AG, Iben JR, Gaidamakov S, Lee J, Hafner M, Maraia RJ.
1290 LARP4 mRNA codon-tRNA match contributes to LARP4 activity for ribosomal protein
1291 mRNA poly (A) tail length protection. Elife. 2017;6:e28889.
1292 68. Mattijssen S, Iben JR, Li T, Coon SL, Maraia RJ. Single molecule poly (A) tail-seq
1293 shows LARP4 opposes deadenylation throughout mRNA lifespan with most impact
1294 on short tails. Elife. 2020;9:e59186.
1295 69. Yang R, Gaidamakov SA, Xie J, Lee J, Martino L, Kozlov G, Crawford AK, Russo AN,
1296 Conte MR, Gehring K, Maraia RJ. La-related protein 4 binds poly (A), interacts with
1297 the poly (A)-binding protein MLLE domain via a variant PAM2w motif, and can
1298 promote mRNA stability. Molecular and cellular biology. 2011;31(3):542-56.
1299 70. Meares GP, Zmijewska AA, Jope RS. HSP105 interacts with GRP78 and GSK3 and
1300 promotes ER stress-induced caspase-3 activation. Cellular signalling.
1301 2008;20(2):347-58.
1302 71. Mkrtchian S, Fang C, Hellman U, Ingelman-Sundberg M. A stress-inducible rat liver
1303 endoplasmic reticulum protein, ERp29. European journal of biochemistry.
1304 1998;251(1-2):304-13.
1305 72. Hotokezaka Y, Katayama I, van Leyen K, Nakamura T. GSK-3β-dependent
1306 downregulation of γ-taxilin and αNAC merge to regulate ER stress responses. Cell
1307 death & disease. 2015;6(4):e1719-.
1308 73. Cairrao F, Santos CC, Le Thomas A, Marsters S, Ashkenazi A, Domingos PM.
1309 Pumilio protects Xbp1 mRNA from regulated Ire1-dependent decay. Nature
1310 Communications. 2022;13(1):1-3.
1311 74. Saeed M, Scheel TK, Gottwein JM, Marukian S, Dustin LB, Bukh J, Rice CM. Efficient
1312 replication of genotype 3a and 4a hepatitis C virus replicons in human hepatoma
1313 cells. Antimicrobial agents and chemotherapy. 2012;56(10):5365-73.
1314 75. Surjit M, Jameel S, Lal SK. The ORF2 protein of hepatitis E virus binds the 5′ region
1315 of viral RNA. Journal of virology. 2004;78(1):320-8.
1316 76. Zuker M. Mfold web server for nucleic acid folding and hybridization prediction.
1317 Nucleic acids research. 2003;31(13):3406-15.
1318 77. Kuleshov MV, Jones MR, Rouillard AD, Fernandez NF, Duan Q, Wang Z, Koplev S,
1319 Jenkins SL, Jagodnik KM, Lachmann A, McDermott MG. Enrichr: a comprehensive
1320 gene set enrichment analysis web server 2016 update. Nucleic acids research.
1321 2016;44(W1):W90-7.

1322

1323 **Supplementary Figures and Tables**

Figure S1

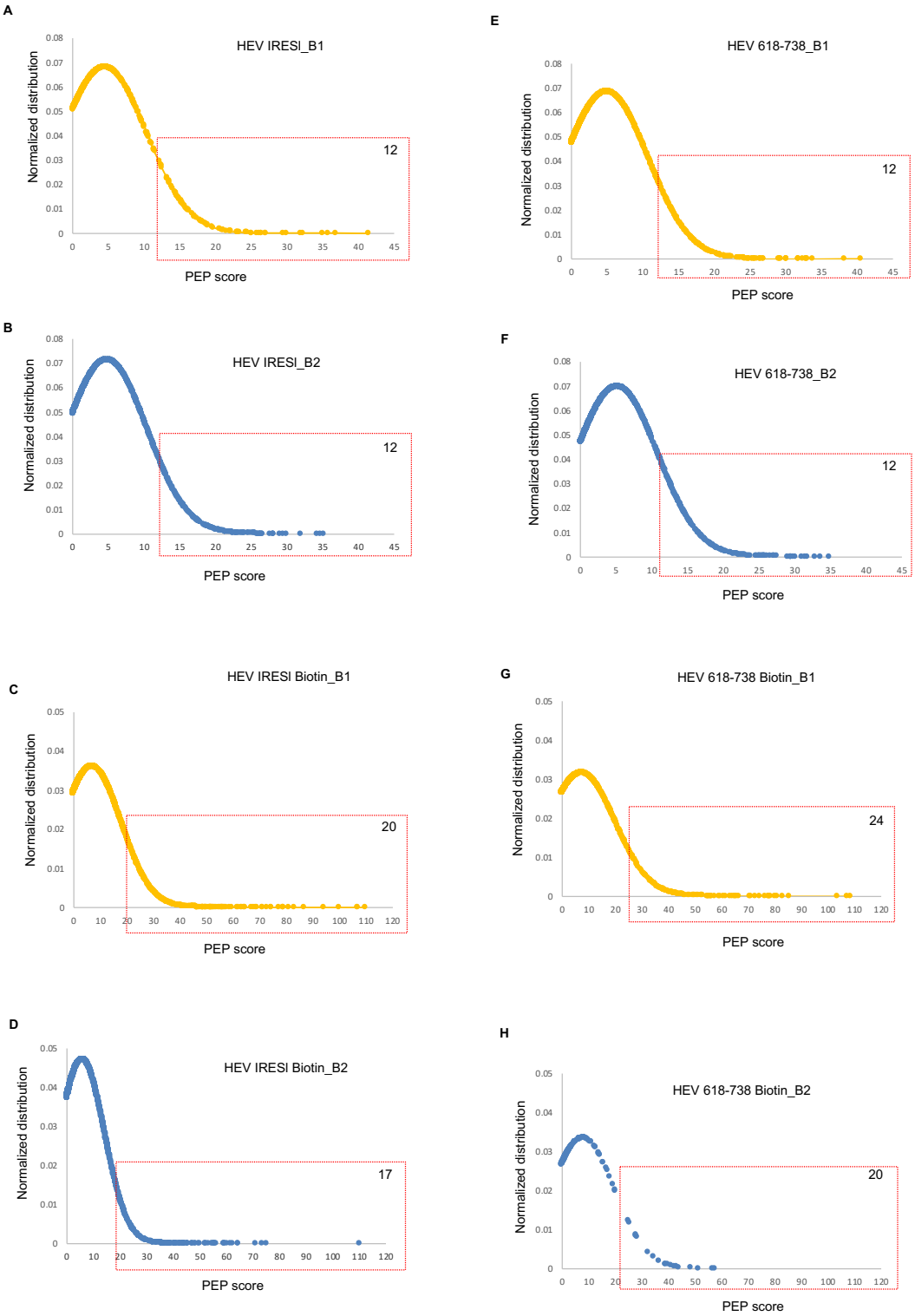

1324

1325 **Figure S1. Normalized distribution plots of the peptides identified by LC-MS/MS.**

1326 (A-H) Normalized distribution plots showing all peptides identified in LC-MS/MS against their
1327 respective PEP scores. B1 and B2 denote biological replicates of the same samples. PEP score
1328 range considered for protein identification is shown by a dotted-lined box.

1329

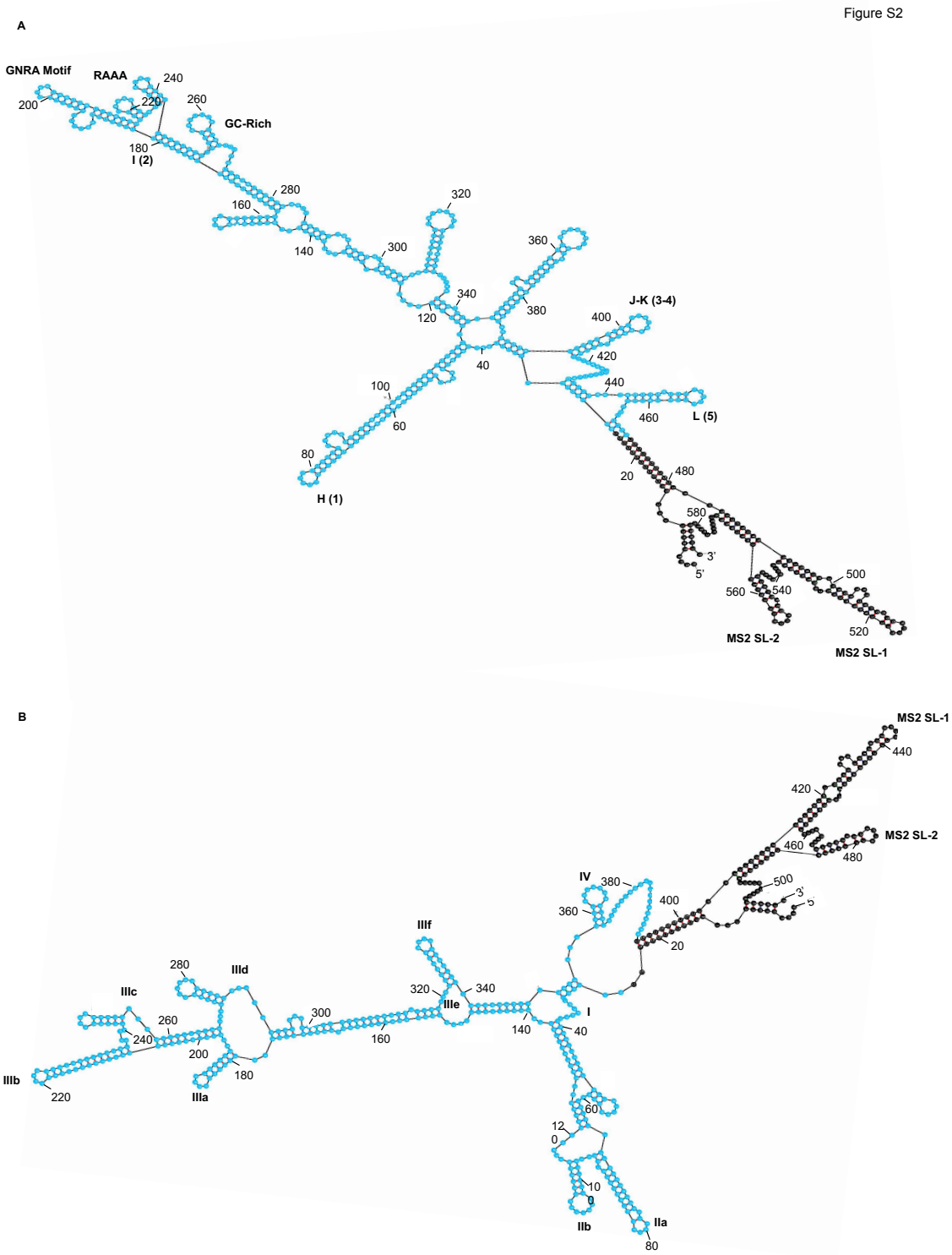

1330

1331 **Figure S2. Predicted secondary structure of the FMDV and HCV IRES RNA.**

1332 (A) Predicted secondary structure of the FMDV IRES RNA (shown in blue) fused to the MS2-
1333 coat protein-binding RNA. MS2 SL-1 and MS2 SL-2 represent MS2 coat proteinbinding RNA

motifs. Five SLs of the IRES are numbered H-L (1-5) and span positions 26113, 114-344, 343-418 and 417- 470, respectively. GNRA, RAAA, GC-rich motifs are as indicated. (B) Predicted secondary structure of the HCV IRES RNA (shown in blue) fused to the MS2-RNA. MS2 SL-1 and MS2 SL-2 represent MS2 coat protein-binding RNA motifs. Four stem-loops (SL) of the IRES are numbered as I, II, III (a-e) and IV.

Figure S3

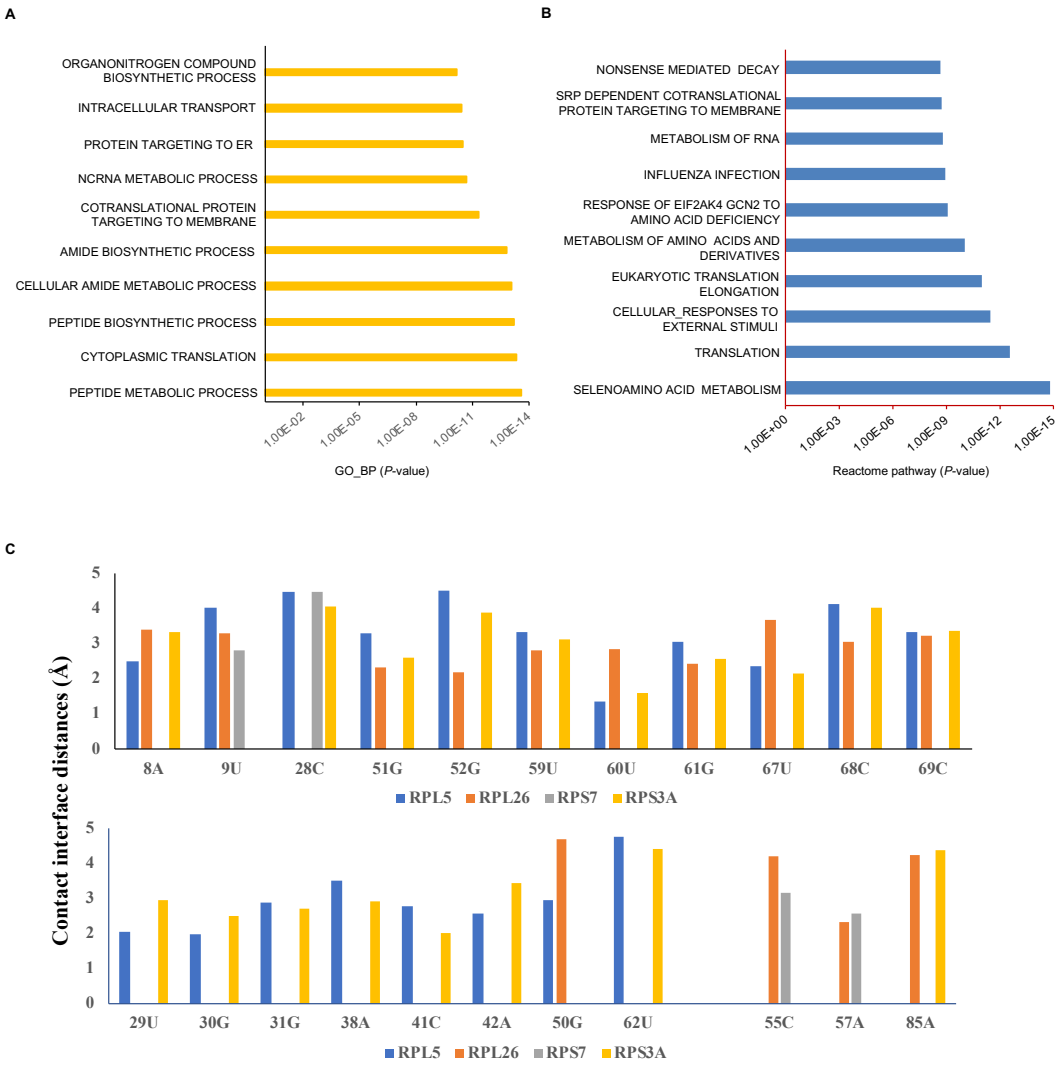

Figure S3. Bioinformatics analysis of the HEV IRESI RNA-host protein interaction.

(A) Graphical representation of the top 10 Biological processes (sorted by P-values) enriched in the HEV IRESI RNA-protein interactome, analyzed by the GSEA tool (B) Graphical

1343 representation of the top 10 Reactome pathways (sorted by P-values) enriched in the HEV
1344 IRESI RNA-protein interactome, analyzed by the GSEA tool. (C) Quantitative pair-wise contact
1345 interface distance calculation between the HEV IRESI RNA and the indicated ribosomal
1346 proteins. The pair-wise interface residues contacts (measured in the form of distance in Å) was
1347 calculated for each complex. The common contact nucleotides of the HEV IRESI RNA are
1348 shown in the upper and lower panels, respectively.

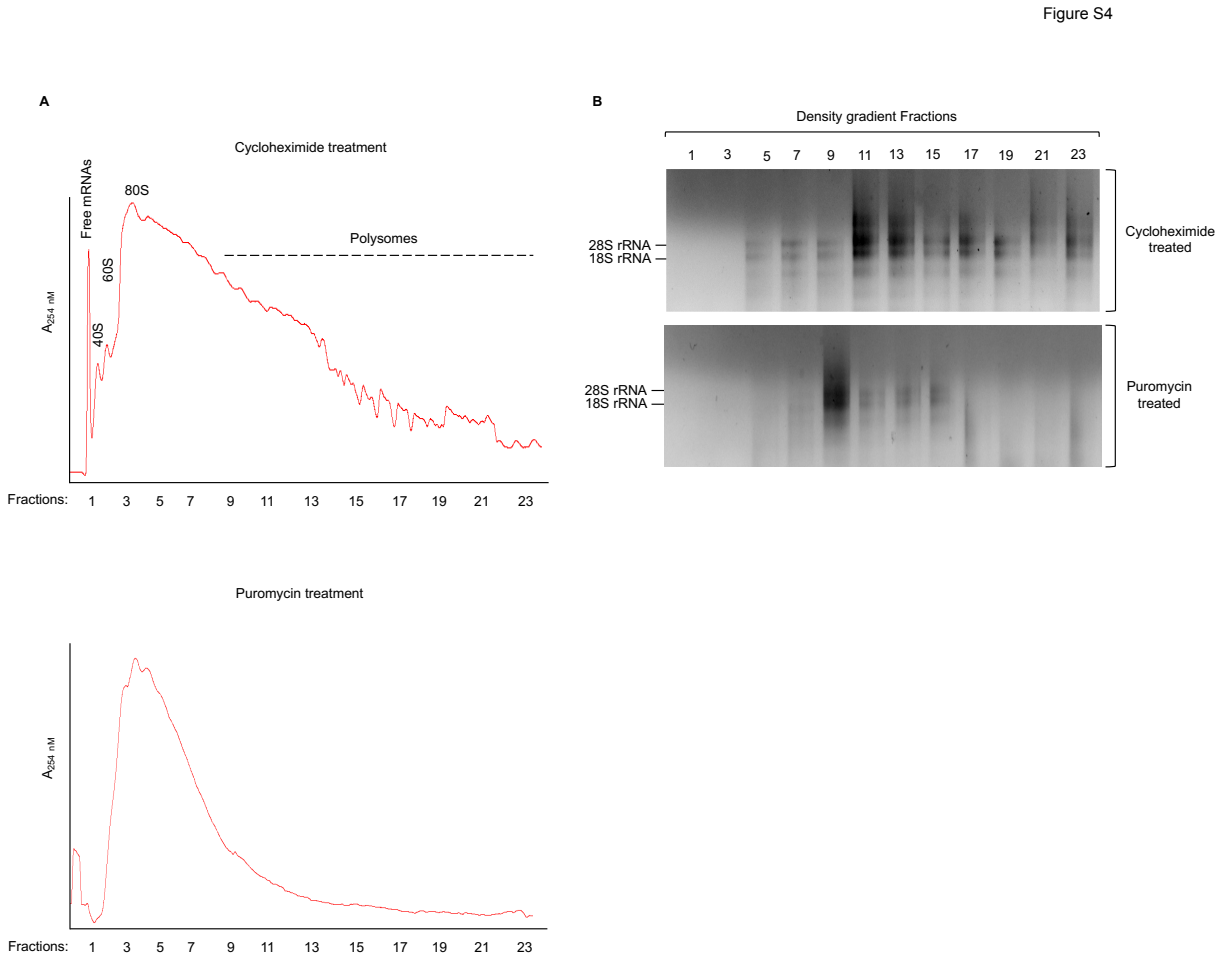

1349

1350

1351 **Figure S4. Ribosome fractionation profiles of cycloheximide or puromycin treated**
1352 **Huh7 cells.**

1353 (A) HEK 293T cells were treated with cycloheximide for 30 min, followed by preparation of the
1354 cytosolic extract and ultracentrifugation on 10-50% sucrose gradients. Equal volume fractions

1355 were collected from the top in an automated fraction collector. Real-time profile of the RNA content
1356 in each fraction was measured at A_{254nm} and the plot generated by the application software is
1357 shown. Peaks corresponding to free mRNAs, 40S, 60S, 80S ribosome and polysome fractions
1358 are indicated based on earlier reports (upper panel). HEK 293T cells were treated with puromycin
1359 for 30 min, followed by preparation of the cytosolic extract and ultracentrifugation on 10-50%
1360 sucrose gradients. Equal volume fractions were collected from the top in an automated fraction
1361 collector. Real-time profile of the RNA content in each fraction was measured at A_{254nm} and the
1362 plot generated by the application software is shown (lower panel). (B) Formaldehyde-agarose gel
1363 electrophoresis of total RNA isolated from the sucrose density gradient fractions of the Huh7 cells,
1364 cotransfected with the pSuper-control RNA plasmid, pSuper-HEV IRESI plasmid and pRL-TK
1365 plasmid and treated with cycloheximide (upper panel) or puromycin (lower panel).

1366

1367

1368

Table S1. List of the HEV IRESI RNA interaction partners, identified by RaPID-LC-MS-MS

Protein name	prot_desc	prot_score	No. of unique peptide	pep_score
EF2	Elongation factor 2	1568	6	59.63
TBA3C	Tubulin alpha-3C/D chain	929	1	24.2
SYTC	Threonyl-tRNA synthetase, cytoplasmic	285	5	17.17
ROA2	Heterogeneous nuclear ribonucleoproteins A2/B1	285	2	35.14
RL7A	60S ribomal protein L7a	262	3	19
BA2L2	Protein BAT2-like 2	75	1	74.55
NUFP2	Nuclear fragile X mental retardation-interacting protein 2	75	1	46.91
SYVC	Valyl-tRNA synthetase	56	8	18.02
DHX9	ATP-dependent RNA helicase A	53	7	42.62
SYTC2	Probable threonyl-tRNA synthetase 2, cytoplasmic	53	5	17.17
ARP19	cAMP-regulated phphoprotein 19	53	1	52.79
ENSA	Alpha-endulfine	53	1	52.79

RL24	60S ribomal protein L24	53	1	35.28
HS105	Heat shock protein 105 kDa	50	6	20.75
CATA	Catalase	49	2	49.14
DDX10	Probable ATP-dependent RNA helicase DDX10	42	9	42.18
LARP4	La-related protein 4	42	1	41.97
MIMIT	Mimitin, mitochondrial	41	1	41.09
DBNL	Drebrin-like protein	39	1	36.56
LBR	Lamin-B receptor	38	1	37.78
AIMP1	Aminoacyl tRNA synthetase complex-interacting multifunctional protein 1	37	3	20.08
NSF	Vesicle-fusing ATPase	37	1	19
VW5B1	von Willebrand factor A domain-containing protein 5B1	35	5	40.75
CEA16	Carcinoembryonic antigen-related cell adhesion molecule 16	35	1	34.88
CCD65	Coiled-coil domain-containing protein 65	34	5	33.67
CN043	Uncharacterized protein C14orf43	34	4	33.93
PUM1	Pumilio homolog 1	34	2	34.22
TXLNG	Gamma-taxilin	33	10	33.34
RFA1	Replication protein A 70 kDa DNA-binding subunit	33	4	32.54
ARSJ	Arylsulfatase J	33	1	32.32
CCD67	Coiled-coil domain-containing protein 67	32	8	32.5
BIVM	Basic immunoglobulin-like variable motif-containing protein	32	3	32.47
YTHD2	YTH domain family protein 2	32	2	32.45
RSBNL	Round spermatid basic protein 1-like protein	32	1	32.09
SPD2A	SH3 and PX domain-containing protein 2A	32	1	31.88
UBAP2	Ubiquitin-associated protein 2	32	1	32.35
GLSK	Glutaminase kidney isoform, mitochondrial	31	1	30.81
MRE11	Double-strand break repair protein MRE11A	31	1	31.09
PRAF3	PRA1 family protein 3	31	1	20.25

CENPP	Centromere protein P	30	1	29.73
ERP29	Endoplasmic reticulum resident protein 29	30	1	23.18
LASP1	LIM and SH3 domain protein 1	30	1	29.73
TM59L	Transmembrane protein 59-like	30	1	29.73
COL10	Collectin-10	29	3	29.32
ZYX	Zyxin	29	2	29.49
GATS	Putative protein GATS	29	1	29.38
PPN	Papilin	29	1	28.77
SC31A	Protein transport protein Sec31A	29	1	29.47
SYQ	Glutaminyl-tRNA synthetase	29	1	29.38
PAPS2	Bifunctional 3~-phphoadenine 5~-phphulfate synthase 2	28	3	27.81
K0649	Protein KIAA0649	28	2	27.59
NUP88	Nuclear pore complex protein Nup88	28	2	25.32
NALDL	N-acetylated-alpha-linked acidic dipeptidase-like protein	28	1	27.97
VPS39	Vam6/Vps39-like protein	28	1	28.29
ZC12C	Probable ribonuclease ZC3H12C	28	1	27.67
LRRF2	Leucine-rich repeat flightless-interacting protein 2	27	5	27.36
M4K4	Mitogen-activated protein kinase kinase kinase kinase 4	27	5	19.92
F195A	Protein FAM195A	27	2	26.9
MDN1	Midasin	26	2	17.57
ACRBP	Acrin-binding protein	26	1	26.38
UBP7	Ubiquitin carboxyl-terminal hydrolase 7	26	1	26.35
GRM7	Metabotropic glutamate receptor 7	25	3	25.19
CHMP5	Charged multivesicular body protein 5	25	1	25.45
MGAP	MAX gene-associated protein	24	13	21.31
ATP7A	Copper-transporting ATPase 1	24	6	24.32
TRM1	N(2),N(2)-dimethylguanine tRNA methyltransferase	24	4	24.25
CND3	Condensin complex subunit 3	24	1	24.31
K2C74	Keratin, type II cytkeletal 74	24	1	23.82
QTRD1	Queuine tRNA-ribyltransferase subunit QTRTD1	24	1	24.1
S28A3	Solute carrier family 28 member 3	24	1	23.51

ZN469	Zinc finger protein 469	24	1	24.29
DYRK3	Dual specificity tyrine-phphorylation-regulated kinase 3	23	1	23.42
EZH1	Histone-lysine N-methyltransferase EZH1	23	1	23.02
EZH2	Histone-lysine N-methyltransferase EZH2	23	1	23.02
FA81A	Protein FAM81A	23	1	22.56
MMP12	Macrophage metalloelastase	23	1	23.36
FA98A	Protein FAM98A	22	5	22.05
XPO4	Exportin-4	22	3	20.68
TEX15	Testis-expressed sequence 15 protein	22	2	21.88
CF050	Uncharacterized protein C6orf50	22	1	22.14
NIN	Ninein	22	1	22.37
VP37A	Vacuolar protein sorting-associated protein 37A	22	1	21.61
CB067	Uncharacterized protein C2orf67	21	10	21.12
EDRF1	Erythroid differentiation-related factor 1	21	8	19.38
YE031	Transmembrane protein ENSP00000382582	21	5	21.06
TT21A	Tetratricopeptide repeat protein 21A	21	4	17.03
ABCG2	ATP-binding cassette sub-family G member 2	21	2	21.29
NMD3B	Glutamate [NMDA] receptor subunit 3B	21	2	20.88
TEX28	Testis-specific protein TEX28	21	2	20.57
ABHD6	Monoacylglycerol lipase ABHD6	21	1	21.27
ACBG2	Long-chain-fatty-acid--CoA ligase ACSBG2	21	1	20.91
COLQ	Acetylcholinesterase collagenic tail peptide	21	1	21.16
GMFB	Glia maturation factor beta	21	1	21.34
NIT1	Nitrilase homolog 1	21	1	21.38
S26A7	Anion exchange transporter	21	1	20.95
YE015	Ankyrin repeat and death domain-containing protein	21	1	24.63
ZN236	Zinc finger protein 236	21	1	20.51
AGAP2	Arf-GAP with GTPase, ANK repeat and PH domain-containing protein 2	20	4	20.09
SYLC	Leucyl-tRNA synthetase, cytoplasmic	20	4	18.18

DC1I1	Cytoplasmic dynein 1 intermediate chain 1	20	2	19.91
HPHL1	Hephaestin-like protein 1	20	2	20.04
MYPC2	Myin-binding protein C, fast-type	20	1	20.25
PRAF2	PRA1 family protein 2	20	1	20.25
CO4A1	Collagen alpha-1(IV) chain	19	9	19.05
PGS2	Decorin	19	5	19.27
RASA1	Ras GTPase-activating protein 1	19	5	19.15
RBL1	Retinoblastoma-like protein 1	19	5	19.69
CO033	Uncharacterized protein C15orf33	19	4	22.99
DYH9	Dynein heavy chain 9, axonemal	18	18	18.01
LKAP	Limkain-b1	18	14	17.68
TRPM3	Transient receptor potential cation channel subfamily M member 3	18	9	22.95
AKT1	RAC-alpha serine/threonine-protein kinase	18	1	17.93
CCD34	Coiled-coil domain-containing protein 34	16	1	20.12
CNN1	Calponin-1	16	1	20.87
KNTC1	Kinetochore-associated protein 1	15	8	18.24

Table S2. Summary of human fetal liver library screening by the Y3H assay to identify the host factors that interact with the HEV IRESI element

Description	No. of Colonies
Number of clones screened	4×10^6
Number of colonies on (LUH^-+10mM 3AT)	395
Number of colonies containing human liver cDNA insert	285
Number of colonies containing unique cDNA insert	75
Unique protein coding sequences in frame with the AD	8
Number of positive clones upon retransformation of the p3HR2-HEV IRESI and the isolated liver library clone	8

1379

Table S3. Analysis of interaction of the HEV IRESI RNA-interacting host proteins (found in Y3H library screening) with the FMDV and HCV IRES RNA[a]

Name of the host protein	HEV IRESI	FMDV IRES	HCV IRES
GREBP	+++	+	+
PPIG	+	-	+++
RPL5	+++	-	+
RPL26	++	-	+++
RPL41	+++	-	-
RPS3A	+++	+++	+++
RPS7	+++	-	+
RPS15A	+++	-	-

[a] +++ : Strong Interaction; + : weak interaction; - : No interaction

1380

1381

1382

1383

1384

1385

1386

1387

1388